The directional energy distribution of wind generated waves as inferred from stereophotographic observations of the sea surface

Proefschrift

ter verkrijging van de graad van doctor in de technische wetenschappen
aan de Technische Hogeschool Delft, op gezag van
de Rector Magnificus prof. ir. B.P.Th. Veltman, voor een
commissie aangewezen door het college van dekanen te verdedigen op
dinsdag 26 mei 1981 te 14.00 uur

door

Leonardus Henricus Holthuijsen
civiel ingenieur

geboren te Amsterdam

Dit proefschrift is goedgekeurd door de promotor
prof. dr. ir. J.A. Battjes

STELLINGEN

I

Golfkomponenten, die door de wind worden opgewekt uit verschillende richtingen, ontwikkelen zich vrijwel onafhankelijk van elkaar.

II

De richtingsverdeling van het energie spectrum van een golfveld dat opgewekt wordt in een situatie waar een konstante wind loodrecht vanaf een rechte kust waait over relatief diep water kan voor veel praktische doeleinden goed benaderd worden met de onderstaande analytische uitdrukking.

$$D(\theta) = A \cos^{2s}(\theta/2)$$

Hierin is $D(\theta)$ de richtingsverdeling met als onafhankelijke variabele de richting θ ten opzichte van de normaal op de kustlijn; A is een normeringscoëfficient en s is een breedte parameter.

III

De voorstellen van Mitsuyasu e.a. (1975) en Hasselmann e.a. (1980) voor de functionele relatie tussen de breedte parameter s van het $\cos^{2s}(\theta/2)$-model voor de richtingsverdeling van het golfenergie spectrum enerzijds en de golffrequentie en de windsnelheid anderzijds verschillen aanmerkelijk van elkaar. De voorkeur dient uit te gaan naar het gebruik van de voorstellen van Hasselmann e.a. (1980) vanwege de kwalitatieve en kwantitatieve superioriteit van de empirische gegevens die gebruikt zijn bij het formuleren van deze voorstellen.

Hasselmann, D.E. e.a. (1980), Directional wave spectra observed during JONSWAP 1973, Journal of Physical Oceanography, Vol. 10, No. 8, blz. 1264-1280

Mitsuyasu, M. e.a. (1975), Observations of the directional spectrum of ocean waves using a cloverleaf buoy, Journal of Physical Oceanography, Vol. 5, No. 4, blz. 750-760

IV

De verschillen tussen het $\cos^{2s}(\theta/2)$-model en de meeste andere één-parameter modellen die in de literatuur zijn voorgesteld voor de richtingsverdeling van het golfenergie spectrum zijn gering indien de kwaliteit en de kwantiteit van de waarnemingen waarop deze voorstellen zijn gebaseerd in beschouwing worden genomen.

V

Het vergelijken van stochastische waarnemingen met modellen kan conceptueel vereenvoudigd worden door de waarnemingen en de modellen voor te stellen als vector verzamelingen in een meer-dimensionale ruimte.

VI

Het is niet waarschijnlijk dat stereofotografie in de nabije toekomst een routine methode zal worden voor het waarnemen van zeegolven.

VII

Het stereofotografisch vastleggen van ruimtelijke golfbeelden in model onderzoek biedt het belangrijke voordeel boven veel andere methoden dat gedetailleerde informatie in sterk gecomprimeerde vorm wordt vastgelegd.

VIII

Het één-parameter golfverwachtingsmodel van Hasselmann e.a. (1976), dat gebaseerd is op vergevorderd fundamenteel onderzoek, verschilt in de uitwerking niet essentieel van het model van Wilson (1965) dat min of meer intuïtief tot stand gekomen is.

Hasselmann, K. e.a. (1976), A parametric wave prediction model, Journal of Physical Oceanography, Vol. 6, No. 2, blz. 200-228

Wilson, B.W. (1965), Numerical prediction of ocean waves in the North Atlantic for December 1959, Deutsche Hydrographische Zeitschrift, Vol. 18, No. 3, blz. 114-130

IX

Het zou de doelmatigheid van het wetenschappelijk onderzoek aan de Nederlandse Universiteiten en Hogescholen ten goede komen indien bij het uitvoeren van dit onderzoek, competitie elementen meer nadrukkelijk tot uiting zouden komen dan thans het geval is. Dit zou onder meer bereikt kunnen worden door in het algemeen een onderzoek project eerst dan te financieren nadat een gedetailleerd schriftelijk voorstel is goedgekeurd door de geldverlenende instantie.

X

De onderzoeker die wetenschappelijk onderzoek verricht voor een opdrachtgever dient te accepteren dat deze bij de begeleiding van dat onderzoek het advies vraagt van een onafhankelijke deskundige.

XI

Een onderzoeker onderschat de mogelijke nadelige gevolgen van zijn onderzoek op de veiligheid van zijn persoon en zijn omgeving meer naarmate zijn persoonlijke betrokkenheid bij dat onderzoek groter is.

XII

Personen die natuurwetenschappelijk onderzoek verrichten in gebieden waar toeristenbelasting verschuldigd is, dienen vrijgesteld te worden van de verplichting tot het betalen daarvan.

XIII

Het gebruik van toiletten met een open afvoer systeem in de West-Europeese treinen is een potentieel gevaar voor de volksgezondheid.

L.H. Holthuijsen
maart, 1981

Contents (concise)

Contents (extended) page

Samenvatting

Het doel van de voorliggende studie is het bepalen van eigenschappen van de richtingsverdeling van de energie van door wind opgewekte golven op basis van waarnemingen met een relatief hoog oplossend vermogen.

Ongeveer 75 waarnemingen van bovengenoemde verdeling zijn geselecteerd uit vijf spectra die verkregen zijn uit stereofotografische opnamen van het zee oppervlak. Drie van deze spectra zijn waargenomen in een situatie die de ideale groei situatie wordt genoemd. Dit is een situatie waar een homogene, stationaire wind loodrecht vanaf een lange rechte kust waait over diep water. De twee andere spectra zijn waargenomen in soortgelijke situaties. Het verschil met de ideale situatie is voor één spectrum dat de windrichting schuin op de kust stond en voor het andere spectrum dat de kustlijn onregelmatig was.

De waargenomen richtingsverdelingen zijn vergeleken met het $\cos^{2s}(\theta/2)$-model dat geïntroduceerd is door Longuet-Higgins e.a. (1963). Doordat de waarnemingen een hoog oplossend vermogen bezitten is het mogelijk de verschillen tussen de waarnemingen en het model te kwantificeren. Het blijkt dat de overeenkomst tussen model en waarnemingen goed is voor veel praktische doeleinden in de ideale groei situatie. Het model is in deze situatie zelfs op een hoog niveau statistisch consistent met die waarnemingen waarvoor een consistentie analyse is uitgevoerd. In de twee andere situaties blijkt de vorm van de richtingsverdeling sterk beïnvloed te zijn door de geometrie van de bovenwindse kustlijn. Dit suggereert een golfgroei waarbij de komponenten uit verschillende richtingen onafhankelijk van elkaar groeien. De resultaten van een eenvoudig parametrisch golfvoorspellings model steunen deze suggestie.

Abstract

The objective of the present study is to determine characteristics of the directional energy distribution of wind generated waves on the basis of observations with a relatively high resolution.

Approximately 75 observations of the above distribution are studied. They are selected from five spectra which are determined from stereophotographic observations of the sea surface. Three of these spectra were obtained in a so-called ideal generation situation. This is a situation where a homogeneous, stationary wind blows perpendicularly off a straight coast over deep water. The other two spectra were observed in similar situations. The difference with the ideal situation is for one spectrum that the wind was slanting across the coastline and for the other that the coastline was irregular.

The observed distributions are compared with the $\cos^{2s}(\theta/2)$-model introduced by Longuet-Higgins et al. (1963). The differences between the observations and this model can be quantified due to the high resolution of the observations. It is found in the ideal situation that the model agrees well for most practical purposes with the observed distributions. In fact, the model is found to be highly consistent with those observations in the ideal situation for which a consistency analysis was carried out. In the other two situations it is found that the shape of the directional energy distribution is strongly influenced by the geometry of the upwind coastline. This suggests a directionally decoupled generation of the waves. The results of a simple parametric wave hindcasting model support this suggestion.

The shape of the observed functional relationship between the width parameter s of the $\cos^{2s}(\theta/2)$-model and the wavenumber agrees fairly well with the shapes suggested by Mitsuyasu et al. (1975) and Hasselmann et al. (1980).

1. Introduction

1.1 Nature and scope

A considerable amount of energy is carried over the ocean surface by waves which are generated by the wind. This flux of energy can be very destructive. To assess the potential danger to man's activities one needs to study such waves. One aspect of such study, the characterization of the directionality of the waves, is the subject of this thesis.

Waves in the ocean can be described on a number of scales. On a very large (oceanic) scale one is interested in the wavefields as they are generated and propagated on the ocean surface. It is usually sufficient in this scale to consider main characteristics of the waves. These vary slowly in place and time. One is thus able to describe the development of the sea state as generated for instance by an atmospheric depression crossing the North Atlantic Ocean. On a smaller scale, and this is the scale with which this thesis is mainly concerned, one would like to describe the wavefield more in detail in a relatively small area, that is, in an area small enough to consider the main characteristics to be constant. The sea surface itself varies wildly in this small area, even within a few seconds or a few meters. To remove this apparent chaos one uses an integral representation of the surface known as the energy spectrum. This spectrum, in its most general form, presents the energy of the waves as a function of frequency, wavenumber and direction.

The spectrum just mentioned is three-dimensional but it can be readily reduced to a two- or one-dimensional spectrum. The most important, or at least the one most often used, is the frequency spectrum. This spectrum has been studied fairly thoroughly by many investigators. It has been observed in a large variety of conditions, difficult to apply laboratory results to the ocean. There are mainly two problems. The first is one of scale: it seems physically impossible to simultaneously scale the spatial dimensions, time, turbulence etc.. This problem seriously hampers present studies of frequency spectra in laboratories. The second problem is that the wind and wave flumes in the laboratories are relatively narrow. Such geometry is not representative for windfields over the ocean. The directional characteristics of wind and waves in a laboratory flume are therefore probably entirely different from those in realistic ocean conditions. For this reason it it not advisable to use the laboratory approach as the prime source of information for the directionality of ocean waves.

In the present study observations were carried out in the oceanic environment, the areas of observation being located in the southern North Sea off the coasts of Holland and Germany. The geophysical conditions were chosen such that the results could be generalized to situations different from those of the observations. The windfields during the observations were fairly homogeneous and stationary, the upwind coast line was either straight or irregular and the water was relatively deep.

The techniques which have been used previously to obtain detailed information of the directionality of ocean waves are based on photography, or radar, or closely spaced wave gauge arrays. The technique chosen for this study is stereophotography. Two synchronized cameras, each carried by a helicopter, were used to take a total of about six hundred stereo photo pairs during a period of three years (1973 - 1976). Each stereo photo pair provides a three-dimensional image of the sea surface as it was at the moment of exposure. Approximately fifty stereo

Other theoretical considerations have been published which are indirectly related to the shape of the two-dimensional spectrum. They are originally due to Hasselmann (1962, 1963). Longuet-Higgins (1976), Fox (1976), Webb (1978) and Dungey and Hui (1979) elaborate on the work of Hasselmann and consider nonlinear wave-wave interactions for narrow spectra which are typical for young sea states. They found that the energy transfer within the spectrum is directed from the peak of the spectrum to lower and higher frequencies, mainly in directions making angles $\tan^{-1}(1/\sqrt{2})$ with the mean direction. The rate of transfer to lower frequencies is slightly greater than that to higher frequencies.

The nonlinear wave-wave interactions have a shape-stabilizing effect on the one-dimensional frequency spectrum (Hasselmann et al., 1973). It is very well possible that they have a similar effect on the two-dimensional wavenumber spectrum. If this were true it would imply that if, for some reason, the shape of the two-dimensional spectrum differs from some standard shape, the nonlinear interactions will redistribute the energy in the spectrum such that the standard shape is attained. It should be noted that this process would only be operative during the generation phase of wave development. Unfortunately, progress in the study of these nonlinear interactions is very slow and no results have been reported in the literature (at least not to the knowledge of the author) which may indicate such stabilizing tendencies as regards the directional characteristics of the two-dimensional spectrum.

The above theories have not resulted in a formulation of main directional characteristics of the wave energy spectrum; observations have provided much more information.

Two kinds of observations can be distinguished. The first kind relates to detailed observations of the directional energy distribution,whereas the symmetrical shape of this function. It has one maximum and it falls off gradually to both sides of this maximum. The coefficients A_1, A_2 and A_3 were estimated from the observations and suggestions were made as to how these coefficients depended on the frequency and the windspeed (although the dependency on the windspeed was not observed).

It appeared from the observations that the relative importance of the $\cos^4\theta$-term in equation (1.2.1) decreases as the frequency increases. The effect of this on the directional distribution is that the width increases as the frequency increases.

The other group of investigators who analyzed the shape of the directional distribution (Tyler et al., 1974) used backscatter of radio waves from the ocean surface in their observations. They obtained ten, extremely detailed, observations of the directional distribution of a wavecomponent of 7 s period on eight consecutive days around Wake Island in the Pacific Ocean. Tyler et al. (1974) judge the observed component to be fully or almost fully developed, that is, the energy density in the frequency spectrum of this component would not increase appreciably with higher windspeed of longer fetch or duration. The component was located on the high frequency side of the peak of the frequency spectrum. Several models for the directional energy distribution were tested and the most satisfactory model turned out to be the following.

$$\hat{D}_o(\theta) = A_4\{\alpha_o + (1 - \alpha_o)\cos^{2s}(\theta/2)\} \qquad (1.2.2)$$

Tyler et al. (1974) judge the difference between the observations and this model to be small, the normalized standard deviation $V_2^{\frac{1}{2}}$, defined in paragraph 3.5.3 being on the order of 0.20. The value of α_0 was small so that for most engineering purposes the following model should be adequate.

The above techniques provide detailed observations. A second kind of observations provides only integral properties of the directional energy distribution. Such properties are for instance a mean direction and a typical width of the directional energy distribution. The observations reported in the literature which are most relevant to the present study were made using records of the vertical motion, the slope and, in some observations, the curvature of the sea surface with a buoy. Shape analysis of the directional energy distribution on the basis of this kind of observations is very limited due to the fact that the directional resolution of the observations is relatively low. But it is possible to indicate whether the observations are consistent with proposed models (Long and Hasselmann, 1979). Such investigations have not been carried out yet but Longuet-Higgins et al. (1963), using a different approach do indicate that the $\cos^{2s}(\theta/2)$-model of equation (1.2.3) agrees better with their observations than do three other models.

The main result of these investigations of integral properties of the directional distribution (as far as they are relevant to the present study) is the numerical value of the width parameter s of the $\cos^{2s}$-$(\theta/2)$-model as a function of frequency and windspeed. Longuet-Higgins et al. (1963), Mitsuyasu et al. (1975), Tyler et al. (1974), and Hasselmann et al. (1980) computed values of s from their observations.

One would perhaps expect systematic dependencies between s and relevant geophysical parameters to exist only in relatively simple meteorological situations such as the ideal situation described above. But referring to the shape-stabilizing influence of the nonlinear interactions in the spectrum (Hasselmann et al., 1973 , Hasselmann et al., 1976) one may also anticipate systematic dependencies for spectra generated in slowly varying windfields. In fact, Hasselmann et al. (1976), argue that the directional distribution function can be regarded in such situations as a function of the nondimensional frequency $\tilde{f}$ with the wave age β as a parameter:

$$\tilde{f} = \frac{f}{f_m} \qquad (1.2.4)$$

a function of $\tilde{f}$. They claim a slightly smaller scatter in their data as compared to using $\hat{f}$ as an independent variable. But the difference seems small and may not be statistically significant.

Mitsuyasu et al. (1975) and Hasselmann et al. (1980) found that the maxium value of s was located at or near the peak frequency and that s decreased as simple power functions of $\tilde{f}$. These authors fitted such functions to their data and suggested that the results be universally applicable to young sea states (wave age $\beta < 1$). The agreement between the results of Mitsuyasu et al. (1975) and Hasselmann et al. (1980) is fair as far as the shape of the functional relationship between s and $\tilde{f}$ is concerned. However, the absolute value of s as a function of wave age β, is greatly different.

The main conclusions from the above review are:

a. Present theoretical considerations in the literature do not lead to a formulation of directional characteristics of the wave spectrum.
b. Nonlinear wave-wave interactions probably force the two-dimensional spectrum of growing sea states into a standard shape.
c. Observations of the directional characteristics of the wave spectrum are scarce and usually not very detailed.
d. Those observations which have been published indicate that in a constant or slowly varying windfield the directional spreading of the spectrum is most narrow at the peak of the spectrum.
e. Detailed observations indicate that the shape of the directional distribution remains unchanged during the phase of exponential growth in the ideal situation. These indications do not agree with the observations and suggestions which are mentioned in point g of this review.
f. Detailed observations carried out in slowly varying wind fields, support the $\cos^{2s}(\theta/2)$-model for the directional distribution.

ture of the sea surface as the record of reflected daylight (Stilwell, 1969; Kasevich et al., 1972). The intensity of daylight reflected from the sea surface depends on the slope of the surface. One can theoretically transform such a picture into a two-dimensional wavenumber spectrum. This transformation seems to be fairly simple under very special conditions of skylight illumination. But in general it requires advanced photographic methods of measuring light intensity distributions both from the sea surface and from the sky. Such methods are usually not readily available.

The second photographic method, stereophotogrammetry, is a conventional method. Since the required facilities were available it is the method chosen for this study. The method is standard in land survey and it is commercially feasible for that purpose. Its use for observations of waves requires some adaptations but these are only practical in nature. They do not concern the basics of the method. The method is described in detail in paragraph 2.2 where it will appear that photography from helicopters was used.

At the initiation of the present study (1972) it seemed that the radar techniques would not be practical within a short period of time. But in the course of this study at least one group of investigators put one such technique at a practical level (Tyler et al., 1974). This approach might have been a feasible alternative for the stereophotogrammetric method had facilities been available.

The field program to obtain the stereo pictures for this study was dominated by the need to perform observations only during specific meteorological and topographical conditions which follow from the scientific requirements of the study. Observations were to be carried out in the ideal situation as described in paragraph 1.2 and in situations deviating from this. These were not the only specifications for the field program.

From these spectra (excluding the test case) it is possible to obtain about seventy-five independent directional distributions with a directional resolution of typically 10^o -20^o. The $\cos^{2s}(\theta/2)$-model, which was introduced earlier, is fitted to the observations with a least-squares technique, and a quantitative measure of the goodness-of-fit of this model to the observations is determined. The statistical consistency between the model and the observations is investigated for one spectrum with a Monte-Carlo method. This method was also used to determine the statistical variability of the observed model parameters (the main direction and the value of s).

1.4 Results

Three spectra were obtained in the ideal situation. The qualification "ideal" is used here although some swell was present. This swell caused one of the spectra to be dropped from the analysis. The locally generated spectra appeared to be essentially unimodal and the directional energy distribution was most narrow near the peak of the spectra. This is in agreement with the literature on this subject. Two more spectra were observed, one in a homogeneous, stationary wind field slanting across a straight coast line and one in a homogeneous, stationary wind field with an irregular upwind coast line (both situations with relatively deep water). The shapes of these two spectra are strongly influenced by the geometry of the upwind coast line. This suggests that wave components from different directions are generated independently from each other (directionally decoupled generation). The results of a simple parametric wave hindcasting model support this suggestion.

The best agreement between the observations and the $\cos^{2s}(\theta/2)$-model is found in the ideal situation. The agreement in the slanting wind situation is only slightly poorer (although the main directions deviate considerably from the wind direction) and the agreement is considered to be

2 Methods of observation

2.1 Introduction

The purpose of this chapter is to describe in detail the method which was used to obtain the wave observations which are the focus of this study. The method is stereophotography from helicopters. Additional observations at sea level (waves, wind and currents) are used to evaluate and interpret those observations but they are conventional and a description of these methods of observation is of secondary importance. It is given in Appendices III and VII.

The stereophotographic technique is dealt with in paragraph 2.2. Although this technique is also rather conventional, existing operational systems could not be used because they are designed to survey stationary objects while the sea surface is a relatively fast moving object. This necessitated the development of a new operational system, which has been an essential effort in the realisation of the present study. The description of the system is therefore rather detailed for such a conventional technique. It will be addressed in paragraph 2.2.5.

2.2 Stereophotography of wind generated waves

2.2.1 Introduction

Stereophotography has a relatively long history in the study of wind generated waves. Schumacher (1939) gives a description of a very early effort (1904) with the cameras mounted on an ocean going ship. Unfortunately, spectral analysis had not entered the field of wave research at that time, and the interpretation of these data, and also other early data, was very limited. Surprisingly many efforts have been made since the experiments in 1904. Platforms for the cameras were landbased to measure waves in situations different from those assumed in this study such as for instance in the surfzone, in a harbour or near breakwaters. The arguments used there would probably be very similar. As a matter of fact a number of stereo pictures of breaking waves has been made over the breakwaters of Rotterdam harbour and even the spray from these breaking waves can be observed in three dimensions in these pictures. The system has also been successfully used to measure waves generated in a hydraulic laboratory.

2.2.2 Basic elements of the system

Some relevant aspects of stereophotogrammetry will be outlined briefly based on Thompson (1966), and some basic system requirements will be indicated.

Principles of stereophotogrammetry

To reduce the system to its most essential structure, it is assumed that the photographs are made looking downwards, that is, the camera axes are truly vertical during the exposure of the film. The image in the photograph will then be a projection of the terrain directly under the camera. The distance between points on the ground at equal elevation can be determined fairly simply if the scale of photography is known. This scale can be expressed in terms of f and h as in equation (2.2.1) where s is the scale, defined as the ratio of corresponding distances in the terrain and in the photograph, f is the focal length of the lens and h is the altitude of photography above the horizontal terrain level ABC (fig. 2.2.1).

$$s = f/h \qquad (2.2.1)$$

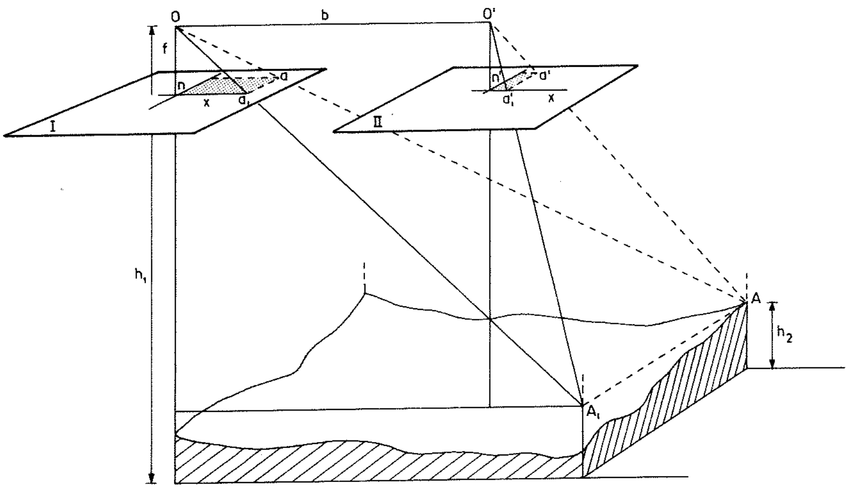

Fig. 2.2.2. Stereo photo pair (after Thompson, 1966).

projections of a and a' on the x-axes are a_1 and a_1', which are the images of A_1. The values of the abcissas na_1 and $n'a_1'$ are different and this difference is by definition the parallax (p) of A for the two pictures. Its value is given in the following equation:

$$p = na_1 - n'a_1' \qquad (2.2.2)$$

It can be shown, using similar triangles, that h_2 is

$$h_2 = h_1 - \frac{bf}{p} \qquad (2.2.3)$$

This equation is the basis of the photogrammetric analysis to determine the elevation of points in the photographed terrain.

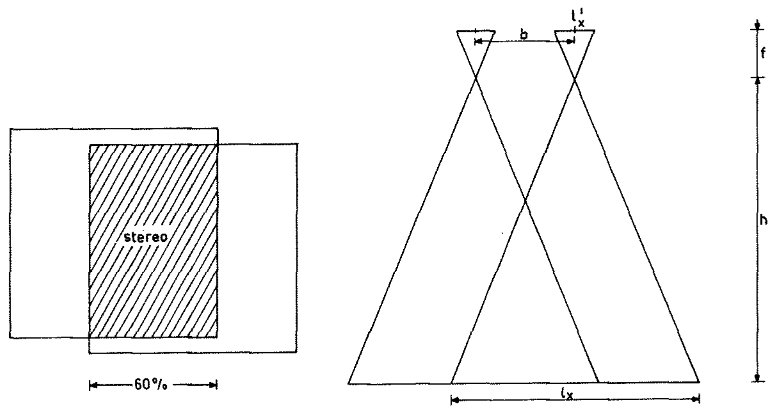

Fig. 2.2.3. Stereophotographic overlap.

The format of the picture in x-direction is l'_x, corresponding to a distance l_x in the terrain. By considering similar triangles in fig. 2.2.3 and by equating b to 0.4 l_x as required for a 60% overlap in x-direction, the following relationship can be found.

$$\frac{h}{b} = \frac{f}{0.4\ l'_x} \qquad (2.2.4)$$

For a given set of cameras with f and l'_x fixed, it appears that the ratio h/b is fixed. This leaves h, the altitude, or b, the distance between the cameras, to be chosen for the actual photographic operations.

The altitude for a photographic mission is chosen on the basis of two considerations. They concern the error in the measurements and the size of the area to be photographed. More information on this subject in terms of spectral parameters is given in Appendix I.

fast flying airplane. Howard (1969) did obtain stereo effects and the pictures were analyzed to produce wave number spectra.

In the present study an effort is made to estimate the maximum permissible time interval. It is difficult to state the problem quantitatively and only an order of magnitude can be established. The measurements in the stereo photographs are based on parallax effects in the images, that is, on horizontal displacements in the pictures. These should solely be the result of the three-dimensional geometry of the surface. But horizontal displacements are also caused by the horizontal or vertical movements of the surface between the two exposures. In particular the horizontal movement was considered to be important since its speed is much greater than that of the vertical movement. It was estimated that a horizontal displacement in the surface of a decimeter, say, would result in an error of a few centimeter in determining the surface elevation from a few hundred meters altitude. This error seems to be acceptable. To correctly establish from this spatial limitation the requirement for the time interval is very complicated because of the random nature of the sea surface. The problem is reduced appreciably if it is assumed that the phase speed of the significant wave can be used to transform the spatial limitations into a time interval. The photographic system has been designed to be used in situations where this phase speed would not exceed 10 m/s (significant period less than 7 s). It follows that in the most unfavourable conditions the above mentioned limit of one decimeter, and consequently the error of a few centimeter, is reached in 10 ms. For good measure the acceptable limit was set at 5 ms. These values are consistent with those mentioned by Cote et al. (1960) and Cruset (1952).

The value of 5 ms seems to be unnessecarily small when compared with the exposure time of the film which is 5 to 10 ms. But the effect of the finite exposure time is to blur the image, whereas differences in timing produce false parallax which can cause larger errors.

wing this interval between triggering and shutter opening will be called camera delay. It consists of an average delay and a random variation which for the purposes of the present study is adequately described by its standard deviation. When two of these cameras are triggered perfectly simultaneously, the film in the two cameras would still be exposed at different times due to the differences in camera delays.

When activating a camera one can conceivably anticipate the moment of exposure from mechanical or electronic indicators in the camera. When the delay in one of the cameras (the shortest delay) is electronically increased to match the delay in the other camera one can obtain synchronized exposures. This approach was seriously considered for cameras with a rotary disc shutter where such an anticipation can be made for each exposure. Synchronization seemed to be attainable by controlling the speed of the rotating discs electronically but major mechanical and electronic adaptations in the cameras would be needed and the proprietors (commercial firms) did not wish to have the cameras adapted to such an extent. Instead a less demanding approach was tried. If the standard deviation of the camera delay could be reduced to an acceptable value (1 or 2 ms, say) only the difference between the average camera delays of the two cameras would need compensation. This has been tried by providing each camera with an electronic unit to generate an additional delay for each camera such that the total average delay in one camera is (almost) equal to that of the other camera. The basic idea is illustrated in fig. 2.2.4 where the time diagram of the sequence is schematically indicated.

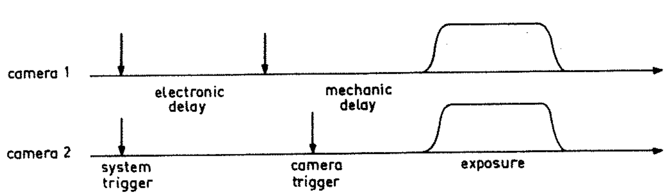

Fig. 2.2.4. Time diagram of camera triggering.

equipment as a radio receiver (to trigger the cameras), suction pump (for flattening the film during exposure) and power supply. Each unit provides support for each of the cameras but a second camera can also be plugged in. It can be triggered simultaneously with the other cameras. The function of this additional camera will be explained later when the problem of determining the scale of photography will be addressed. For a detailed description reference is made to v.d. Vliet (1972,1974).

The equipment was tested extensively both in the laboratory and during testflights (5 flights in all, each with approximately 60 exposures). During the first flight with the Hasselblads, the cameras were mounted outside the aircraft. This mounting proved to be unsatisfactory because the camera delays grew to unacceptable values during the flight. These delays could be measured during the flights through the use of a flash gun contact on the cameras which closed at the initiation of the exposure. To find the cause of the unstable character of the camera delays, the cameras were tested in the laboratory and it was found that the camera delays were sensitive to changes in temperature and humidity. To avoid this problem, the cameras were mounted inside the aircraft and sealed from the outside air by a window pane of optical glass. The Hasselblad cameras have performed perfectly ever since. The same type of mounting was used for the UMK cameras. These cameras, however, failed to perform from time to time due to failures of electronical or mechanical parts inside the cameras. These failures could not always be traced or repaired during the photographic missions and some missions have had to be abandoned. It should perhaps be restated in this context that the cameras have not been specifically designed for survey photography from aircraft and that they have been subject to conditions which are probably far outside the manufacturer's specifications (e.g. excessive vibrations, see the third section of this paragraph on camera mounting).

to know the position with an accuracy consistent with the variations of characteristic parameters of the wave field. The orientation of the helicopters is needed to determine the orientation of the pictures relative to the wind direction. An average deviation of 5^{o} and a standard deviation of 5^{o} in the helicopter orientation seems to be acceptable for this purpose.

Camera mounting

The helicopters were accomodated with drop doors. These were open during the photographic missions and the cameras were mounted over these doors on a wooden plank. As noted before, a window pane of optical glass sealed the cameras from the outside air. It was found during the test flights that the floor of the helicopter tilted approximately 7^{o} (head down) at a forward speed of about 70 knots which was a typical speed for all operations. For convenience in the analysis of the pictures this tilt was removed from the cameras by tilting the mountings. The cameras were secured with bolts and nuts to the wooden plank which in turn was bolted down to the helicopter floor. A consequence of this construction was that the motion of the helicopter, including vibrations, were transmitted directly to the cameras. A gyro-stabilized and vibration-damping construction was considered but the cost was prohibitive.

In addition to the two downward looking cameras (one in each helicopter), a third camera was introduced. This camera was used for two purposes both related to estimating the distance between the helicopters: maintaining the helicopter formation and determining the scale of photography.

In conventional aerial survey the scale of photography is usually determined from known distances in the photographs between points in

	Average	Standard deviation
altitude difference	10.6%	1.6% (of altitude)
overlap of pictures in x-direction	60%	9.5%
overlap of pictures in y-directions	79%	6.5%
tilt	1.9^{o}	2.1^{o}
difference in orientation	5.6^{o}	4.7^{o}

Table 2.2.2. Observation of camera position and orientation (see also table 2.2.1).

The numbers in this table are based on approximately thirty observations except those for the difference in orientation which are based on ten observations. The average deviation of the helicopter orientation relative to its desired orientation was 1.5^{o}. The standard deviation of the helicopter yaw was 3.3^{o} (σ_{yaw} = 0.06 radians). These values were based on ten observations over a fixed platform at sea with known orientation.

2.2.4 Operational procedures

The operational procedures were of two kinds: those related to the preparations for the photographic mission and those related to the actual flight. As regards the preparations it may suffice to indicate that the logistics were mostly arranged through military channels. Details on these arrangements, including transportation, housing, licences etc. (areas of operation in Holland and Germany) do not seem to be relevant here. The preparation of the photographic equipment was limited to setting the instrumentation on stand-by with a film type depending on anticipated weather conditions. During the actual flight attention was concentrated on the second kind of procedures which will be discussed next.

given set of cameras depended on several considerations related to the wave field. These considerations and the results thereof are discussed in Appendix I.

When the required helicopter formation was achieved, the photographer started the photographic sequence by operating the radio transmitter. Careful timing located the pictures within a few hundred meter of the specified postion. But the operational procedures were often frustrated by camera failures, atmospheric disturbances clouds, rain etc. and sorties have had to be relocated, flown again or abandoned.

2.2.5 Photogrammetric analysis

To quantify the information of the stereo photo pairs, equation (2.2.3) is evaluated for each point of interest of the sea surface. In this equation the values of b (the camera distance) and f (the focal length of the lens) are known, h (the altitude) can be chosen arbitrarily as elevations are taken relative to an arbitrary level of references. The parallax p is determined from the pictures.

Determining the parallax of a point requires the identification of two images of one point, one image in the lefthand picture and one in the righthand picture. These two points in the pictures are called homologous points. In conventional stereophotographic survey (land terrain) the identification of the homologous points is relatively easy through visual inspection of the pictures separately. If homologous points are not so easy to identify or if the number of points of interest is great, some degree of automation is called for. The identification is then basically carried out by a correlation technique.

Two processes can be used to carry out the correlation. The first technique will be indicated only briefly because if was not used in this

Having made the identification, the positions of the dots in the pictures determine the parallax, and the coordinates of the point in the three-dimensional space are recorded.

A cartesian system of x, y and z coordinates was defined in the three-dimensional space created in the stereoscopic viewing device. The x- and y-axes defined the horizontal plane and the z-axis was pointing upward. The operator was asked to determine the sea surface elevation on a square grid in a region as large as possible. In the pictures of the UMK cameras the region of overlap is usually a square due to the overlap percentage and the format size of the pictures. In the pictures of the Hasselblad cameras the region was oblong for the same reasons and the operator was asked to analyze only the largest possible square from the total region available.

The mode of operation was a profiling method: the sea surface was scanned along the gridlines parallel to the y-axis (which pointed into the flight direction). While the x- and y-position was controlled automatically, the operator controlled the vertical position of the floating point which followed the sea surface as closely as possible. Every time the horizontal position of the floating point crossed a gridpoint the three coordinates of that point were recorded on tape. In some instances the surface could not be percieved with any accuracy (loss of stereoscopy due to photo quality, sun-glitter etc.). The gridpoints concerned were either labelled or skipped.

The analysis of each picture resulted in a set of observations of the elevation of the sea surface relative to an arbitrary frame of reference. This set is given symbolically as

$$\tilde{\eta}' = \tilde{\eta}'(x_i, y_j) \qquad (2.2.5)$$

the stereophotogrammetric information is available. This is due to the fact that squares from one sortie should have one common size which is not always chosen to be the smallest available in a sortie. The regions where stereo information is missing are filled with extremely high values for η'. This action causes these regions to be treated as gaps (see point b).

b. At the positions where observations of the surface elevation are missing or not realistic, zero's are inserted. The manner is which this is done is discussed below.

c. The surface elevation should have its two-dimensional linear trend removed. This is done such that the positions identified in point b are not considered. The surface elevation (after removing the linear trend) is set equal to zero at these positions.

Before removing the two dimensional linear trend, spikes and gaps in the photogrammetric results are identified (point b). That is, locations in the grid where the surface data fail to pass a test are rejected from the analysis. This test is essentially one-dimensional in nature but it is applied in two directions: the x- and y-direction. Consider one row of data points (e.g. y-value constant) in an analyzed region.Usually this series of data points has a small but significant linear trend and it may contain spikes or gaps (fig. 2.2.7).

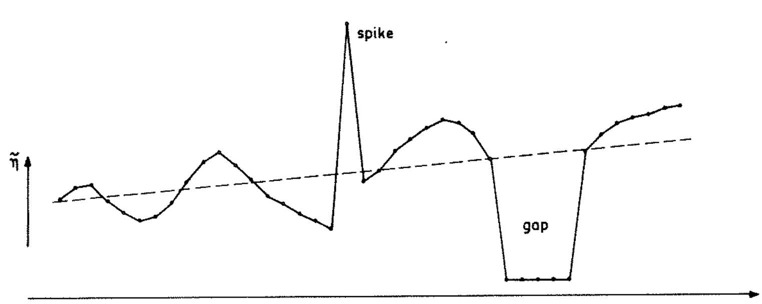

Fig. 2.2.7. Spikes and gaps in sequence of data points.

The function to be minimized is given in the following equation.

$$V = \sum_{i=1}^{m} \sum_{j=1}^{n} \{\tilde{\eta}(x_i, y_j)\}^2 = \sum_{i=1}^{m} \sum_{j=1}^{n} \{\tilde{\eta}'(x_i, y_j) - ax_i - by_j - c\}^2 \tag{2.2.7}$$

where *m* and *n* are the maximum number of data points in x- and y-direction respectively. The minimization results in the following matrix.

$$\begin{vmatrix} \sum_{i=1}^{m}\sum_{j=1}^{n} x_i^2 & \sum_{i=1}^{m}\sum_{j=1}^{n} x_i y_j & \sum_{i=1}^{m}\sum_{j=1}^{n} x_i \\ \sum_{i=1}^{m}\sum_{j=1}^{n} x_i y_j & \sum_{i=1}^{m}\sum_{j=1}^{n} y_j^2 & \sum_{i=1}^{m}\sum_{j=1}^{n} y_j \\ \sum_{i=1}^{m}\sum_{j=1}^{n} x_i & \sum_{i=1}^{m}\sum_{j=1}^{n} y_j & \sum_{i=1}^{m}\sum_{j=1}^{n} 1 \end{vmatrix} \times \begin{vmatrix} a \\ b \\ c \end{vmatrix} = \begin{vmatrix} \sum_{i=1}^{m}\sum_{j=1}^{n} \tilde{\eta}'(x_i, y_j) x_i \\ \sum_{i=1}^{m}\sum_{j=1}^{n} \tilde{\eta}'(x_i, y_j) y_j \\ \sum_{i=1}^{m}\sum_{j=1}^{n} \tilde{\eta}'(x_i, y_j) \end{vmatrix}$$

The data points labelled "spike" or "gap" are excluded from the summation terms in the matrix. It may be pointed out that if no data excluded from the summation, the terms in the matrix can be replaced by analytical expressions for the sum. This simplified matrix is given below. It is identical to the one given in Cote et al. (1960).

$$\begin{vmatrix} \frac{mn(n-1)(2n-1)}{6} & \frac{mn(n-1)(m-1)}{4} & \frac{mn(n-1)}{2} \\ \frac{mn(n-1)(m-1)}{4} & \frac{nm(m-1)(2m-1)}{6} & \frac{nm(m-1)}{2} \\ \frac{mn(n-1)}{2} & \frac{nm(m-1)}{2} & \frac{nm}{1} \end{vmatrix} \times \begin{vmatrix} a \\ b \\ c \end{vmatrix} = \begin{vmatrix} \sum_{i=1}^{m}\sum_{j=1}^{n} \tilde{\eta}'(x_i, y_j) x_i \\ \sum_{i=1}^{m}\sum_{j=1}^{n} \tilde{\eta}'(x_i, y_j) y_j \\ \sum_{i=1}^{m}\sum_{j=1}^{n} \tilde{\eta}'(x_i, y_j) \end{vmatrix}$$

3. Methods of analysis

3.1 Introduction

The purpose of this chapter is to give a detailed description of the methods which are used to analyze the stereophotogrammetric results. The analyses of the observations at sea level (waves, wind and currents) are conventional and of secondary importance. The description of these analyses is given in Appendices III and VII.

Before entering into a detailed description of the analysis of the stereophotogrammetric results some definitions and concepts are introduced in the next paragraph, where attention is directed towards the spectral description of the moving sea surface. This description requires the definition of a three-dimensional spectrum; one dimension is related to time and two dimensions are related to the horizontal plane (e.g. wavelength and direction). The number of dimensions can be reduced to two without loss of information if the linear theory of surface gravity waves is applicable. This number can be reduced to one if directional information is not required. One can thus define several types of spectra depending on which of the dimensions are chosen to remain. The interrelations between these spectra are described here because the results of the present study and the information in the literature have been expressed in terms of these spectra.

In the analysis of the shape of the observed directional distributions, a model is fitted to the observations. It is possible to carry out rather detailed comparisons between this model and the observations, as the observations are obtained with a relatively high resolution. The methods which are used, are described in paragraph 3.5.

Consider the sea surface elevation as a function of place and time to be Gaussian distributed with zero mean. Its statistics can then be completely described by the following three-dimensional covariance function :

$$C(\vec{r},\tau) = < \eta(\vec{x},t)\eta(\vec{x} + \vec{r},t + \tau) > \qquad (3.2.1)$$

In this equation C is the covariance, $\vec{r}$ is a displacement vector and τ is a time lag, < > indicates ensemble averaging. The function $C(\vec{r},\tau)$ gives the variance of the elevation η and the statistical dependence between surface elevations at any two points in time and space. It is potentially a useful function to study wind generated waves as it describes the statistics of $\eta(\vec{x},t)$ completely. However, many problems are studied more conviently in the realm of the spectrum which is the Fourier transform of the covariance function :

$$E_o(\vec{k},f) = \iiint_{-\infty}^{\infty} C(\vec{r},\tau)e^{-i2\pi(\vec{k}.\vec{r} + f\tau)}d\vec{r}\, d\tau \qquad (3.2.2)$$

E_o is the three-dimensional variance density spectrum, $\vec{k}$ is the wave-number vector and f is the frequency. The purpose of using the subscript $_o$ will become evident later in this paragraph. The Fourier transform is reversible, implying that the spectrum contains as much information on the elevation $\eta(\vec{x},t)$ as does the covariance function. The total variance (σ_η^2) or energy of the waves is equal to $C(\vec{0},0)$ which is equal to the following integral of the spectrum :

$$\sigma_\eta^2 = \iiint_{-\infty}^{\infty} E_o(\vec{k},f)\, d\vec{k}\, df \qquad (3.2.3)$$

The variance density is closely related to the energy density, the difference being a constant factor ρg. This close relatioship indicates that interpretations and manipulations of the spectrum are more physical

It follows from equations (3.2.4), (3.2.6) and (3.2.7) that $E(k,\theta)$ and $E(\vec{k})$ are related as

$$E(k,\theta) = E(\vec{k})\, J_1 \qquad (3.2.8)$$

Note that in the integrations in equations (3.2.4) and (3.2.7) the discrimination between components traveling in opposite directions has been lost. The basic reason is that temporal information has been removed by the integrations. In the integration in equations (3.2.4), $E_o(\vec{k},f)$ and $E_o(\vec{k},-f)$ are superimposed because $E_o(\vec{k},f)$ is an even function. This implies that $E_o(\vec{k},f)$ and $E(-\vec{k},f)$, the energy densities of components traveling in opposite directions, are superimposed. This results in the 180^o ambiguity in the direction of propagation. A different spectrum $E_o(\vec{k})$ is therefore introduced which will maintain the 180^o discrimination. Its definition is

$$E_o(\vec{k}) = 2\int_0^\infty E_o(\vec{k},f)\, df \qquad (3.2.9)$$

The function of the subscript $_o$ may now be evident. It serves to indicate whether the spectrum contains the 180^oambiguity or not. The relationship between $E_o(\vec{k})$ and $E(\vec{k})$ is given below.

$$E(\vec{k}) = \tfrac{1}{2}\{E_o(\vec{k}) + E_o(-\vec{k})\} \qquad (3.2.10)$$

Analogous to $E(k,\theta)$, $E_o(k,\theta)$ can be defined as in equation (3.2.11) and its relation to $E_o(\vec{k})$ is given in equation (3.2.12)

$$E_o(k,\theta) = 2\int_0^\infty E_o(k,\theta,f)\, df \qquad (3.2.11)$$

$$E_o(k,\theta) = E_o(\vec{k})\, J_1 \qquad (3.2.12)$$

The relationship between $E_o(k,\theta)$ and $E(k,\theta)$ is given in the next over frequency and direction. Its definition is given below.

$$E_o(f,\theta) = 2 \int_0^\infty E_o(k,\theta,f)\, dk \qquad \text{for} \quad f \geqslant 0 \qquad (3.2.19)$$

It is a hybrid spectrum in the sense that it combines information on the temporal behaviour with information on the spatial behaviour of the sea surface. It follows from equations (3.2.6), (3.2.17) and (3.2.19) that E(f) can be determined from $E_o(f,\theta)$ according to equation (3.2.20).

$$E(f) = \int_0^{2\pi} E_o(f,\theta)\, d\theta \qquad \text{for} \quad f \geqslant 0 \qquad (3.2.20)$$

According to the linear theory of surface gravity water waves the wavenumber k and the frequency f are related. This relationship is dependent on the waterdepth d and a mean current velocity $\vec{V}$. The relationship, called the linear dispersion relationship, is given in equation (3.2.21) where f is the frequency as observed in a system stationary with respect to the sea bottom.

$$f = \left\{\frac{gk}{2\pi} \tanh(2\pi kd)\right\}^{\frac{1}{2}} + \vec{k}.\vec{V} \qquad (3.2.21)$$

It follows from this relationship that the value of $E_o(\vec{k},f)$ is non-zero only at the surface in $(\vec{k},f)$- space created by the dispersion relationship, thereby reducing the number of independent variables from three to two. For actual waves the location of the energy is not restricted to this surface due to nonlinearities. For the local description of the wavefield these nonlinearities are insignificant (at least for deep water). It also follows that $E_o(f,\theta)$ can be expressed in terms of $E_o(\vec{k})$ as in equation (3.2.22).

$$E_o(f,\theta) = E_o(\vec{k})\; J_2 \qquad (3.2.22)$$

$$\int_0^{2\pi} D_o(\theta;k) = 1 \tag{3.2.29}$$

$$\int_0^{2\pi} D_o(\theta;f) = 1 \tag{3.2.30}$$

It also follows that $D(\theta;k)$ includes the 180^o-ambiguity of $E(k,\theta)$ resulting in the following relationship between $D(\theta;k)$ and $D_o(\theta;k)$.

$$D(\theta;k) = \tfrac{1}{2}\{D_o(\theta;k) + D_o(\theta + \pi;k)\} \tag{3.2.31}$$

If the current velocity $\vec{V}$ is zero, the Jacobian J_2 of equations (3.2.22) and (3.2.23) is independent of the direction θ. One of the consequences in that case is that $D_o(\theta;k)$ is equal to $D_o(\theta;f)$ for corresponding values of f and k (equation (3.2.21)). Another consequence is that the one-dimensional wavenumber spectrum $E(k)$ and the frequency spectrum $E(f)$ are directly related as in the next equation.

$$E(k) = E(f)\,\frac{J_1}{J_2} = E(f)\,\frac{df}{dk} \tag{3.2.32}$$

The above spectra and distributions are the ones most commonly used in the literature on wave research and they will be used in the following. One distribution which is not very common but which does fit in logically is

$$D_o^*(\theta) = \int_0^{\infty} E_o(k,\theta)\, dk \tag{3.2.33}$$

This function $D_o^*(\theta)$ should be called the directional spectrum as it gives the distribution of the wave energy as a function of direction in analogy with the frequency spectrum which gives the wave energy as a function of frequency. However, this name is usually reserved in the literature for one of the two-dimensional spectra (although there is no consensus on which one). To avoid confusion, the term "directional spectrum" will not be used in this thesis.

A number of N stereo picture pairs (typically 10) is analyzed for each sortie. Each of these picture pairs provides a sample of the sea surface elevation as a function of horizontal coordinates in a region of dimensions $L_x \times L_y$. The samples from one sortie are indicated in the diagram as ${}^1\tilde{\eta}(\vec{x})$, ${}^2\tilde{\eta}(\vec{x})$ etc. Each of these samples is Fourier-transformed to obtain raw estimates of the two-dimensional wavenumber spectrum with resolution of $(L_x \times L_y)^{-1}$. In the diagram these spectra are indicated as ${}^1\tilde{E}(\vec{k})$, ${}^2\tilde{E}(\vec{k})$ etc. The reliability of these spectral estimates individually is very poor and they are therefore averaged over the N samples (while maintaining the same resolution) to arrive at a more reliable estimate, $\tilde{E}(\vec{k})$. This estimate is transformed to the (k,θ) domain, resulting in the spectrum $\tilde{E}(k,\theta)$. From this spectrum the directional distribution is determined as a function of the wavenumber, $\tilde{D}(\theta;k)$. A model for the directional distribution is fitted to these observations, resulting in estimates of a width parameter s and a main direction $\overline{\theta}$ as a function of wavenumber. The goodness-of-fit of the model to the observation is quantified for each spectrum in two relative residuals V_2 and V_5. For one spectrum the statistics are determined of the model parameters s and $\overline{\theta}$ and of the relative residual V_2. The frequency spectrum $\tilde{E}(f)$ is computed from $\tilde{E}(k,\theta)$ by transformation from the (k,θ) domain to the frequency domain.

The steps outlined above are described fully in what follows.

The determination of spectra is often directly based on the formal definition of the spectrum, that is, it is often calculated by Fourier-transforming the covariance function (equations (3.2.5) and (3.2.18)). During the past 10-15 years an alternate method has been proven to be more efficient on a digital computer. This method is based on the Fast Fourier Transform (e.g. Cooley and Tukey, 1967) of the data without using the covariance function as an intermediate. The actual numerical

The effect of the limited dimensions of the area in which $\tilde{\eta}(\vec{x})$ is available can be evaluated by considering $\eta(\vec{x})$ multiplied with the boxcar function $b_1(\vec{x})$ of the next equation.

$$\left.\begin{aligned} b_1(\vec{x}) &= 1 \text{ for } 0 < x < L_x \text{ and } 0 < y < L_y \\ &= 0 \text{ elsewhere} \end{aligned}\right\} \qquad (3.3.5)$$

The spectrum $\tilde{E}(\vec{k})$ of the resulting function is the spectrum of $\eta(\vec{x})$ convolved with the spectrum of $b_1(\vec{x})$,

$$\tilde{E}(\vec{k}) = E(\vec{k}) \otimes B_1(\vec{k}) \qquad (3.3.6)$$

$B_1(\vec{k})$ is the squared Fourier transform of $b_1(\vec{x})$ which is the damped sine-function,

$$B_1(k_x, k_y) = \frac{\sin(\pi k_x L_x)}{\pi k_x} \; \frac{\sin(\pi k_y L_y)}{\pi k_y} \qquad (3.3.7)$$

The influence of replacing $\tilde{\eta}(\vec{x})$ with zeros at some gridpoints can be established by considering these replacements as aberrations from the boxcar function $b_1(\vec{x})$. The corresponding influence on the wavenumber spectrum is seen as aberrations from $\tilde{E}(\vec{k})$ in equation (3.3.6). But the number of zeros in the observations of this study is small (less than 6% of the total number of data points for each spectrum) and the aberrations are insignificant compared to the influences of $b_1(\vec{x})$. The effect of zero-replacement on the shape of the spectrum is therefore ignored.

The fact that $\eta(\vec{x})$ is only estimated at a regular grid of $\vec{x}$-values can be accounted for by considering the observations to be equal to the function $\eta(\vec{x})$ multiplied by a set of delta functions on the grid of the observations. This set of delta functions is indicated in the next equation.

$$\tilde{E}(\vec{k}) = E(\vec{k}) + E_\varepsilon(\vec{k}) \qquad (3.3.14)$$

where $E_\varepsilon(\vec{k})$ is the noise spectrum. Unfortunately $E_\varepsilon(\vec{k})$ could not be determined in the present study. Only a rough estimate of the total variance of the noise was made (σ_ε^2, Appendix I) and the shape of $E_\varepsilon(\vec{k})$ could only be speculated upon through some conspicuous shape characteristics of the observed wavenumber spectrum $\tilde{E}(\vec{k})$. This will be commented upon in chapter 4 where the observed spectra are presented.

The Fourier transform of the photogrammetric data was carried out with the multi-dimensional, mixed-radix Fast Fourier Transform procedure published by Singleton (1969). For each stereo photo pair estimates of $E(\vec{k})$ were thus determined on a regular grid in $\vec{k}$-space with mesh-sizes Δk_x and Δk_y as given in the following equations.

$$\Delta k_x = 1/L_x \qquad (3.3.15)$$

$$\Delta k_y = 1/L_y \qquad (3.3.16)$$

The ensemble average needed to determine the estimate of the wavenumber spectrum according to equation (3.3.1) is approximated by taking the average of the set of N "raw" spectra,

$$\tilde{E}(k_i,k_j) = \frac{1}{N} \sum_{n=1}^{N} {}^{n}\tilde{E}(k_i,k_j) \qquad (3.3.17)$$

${}^{n}\tilde{E}(k_i,k_j)$ is the "raw" wavenumber spectrum from one stereo photo pair. Each of the "raw" spectra is statistically independent from every other "raw" spectrum. The set of N "raw" spectra obtained after the Fourier analysis is only a sample from all possible "raw" spectra, and the average of the N "raw" spectra is consequently subject to sample variability. This statistical aspect of the observed spectra is addressed in paragraph 4.4 along with resolution aspects.

interpolation. To describe this interpolation let the projected point be (k_r,k_s), fig. 3.3.2, and let the surrounding four points of the grid be (k_i,k_j), (k_{i+1},k_j), (k_i,k_{j+1}) and (k_{i+1},k_{j+1}).

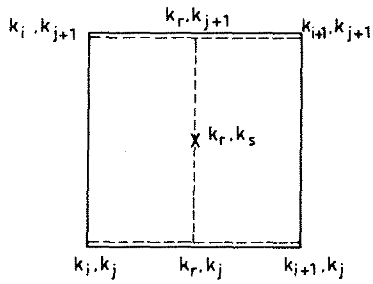

Fig. 3.3.2. Two-dimensional linear interpolation.

The value of $\tilde{E}(k_r,k_s)$ is taken as the linear interpolation of $\tilde{E}(k_r,k_j)$ and $\tilde{E}(k_r,k_{j+1})$. The required value of $\tilde{E}(k_r,k_j)$ results from a linear interpolation of $\tilde{E}(k_i,k_j)$ and $\tilde{E}(k_{i+1},k_j)$, and the required value of $\tilde{E}(k_r,k_{j+1})$ results similarly from $\tilde{E}(k_i,k_{j+1})$ and $\tilde{E}(k_{i+1},k_{j+1})$. The Jacobian used in the transformation is equal to k, in accordance with equation (3.2.8).

The resulting two-dimensional spectrum $\tilde{E}(k,\theta)$ is used to determine the directional distribution $\tilde{D}(\theta;k)$. The transformation given in equation (3.2.25) is carried out at each of the gridpoints of $\tilde{E}(k,\theta)$ by evaluating equation (3.3.21) where $\tilde{E}(k)$ is obtained by integrating $\tilde{E}(k,\theta)$ over the directional range from 0 to 2π.

$$\tilde{D}(\theta;k) = \frac{\tilde{E}(k,\theta)}{\tilde{E}(k)} \qquad (3.3.21)$$

The frequency spectrum E(f) cannot be determined from spatial recordings of the sea surface and current observations because it requires esti-

3.4 Spectral resolution and reliability

The results of the stereophotographic observations have been expressed in the preceding paragraph in terms of the two-dimensional wavenumber spectrum, the directional distribution as a function of wavenumber and the frequency spectrum. To determine the statistical significance of these functions both the statistical reliability and the resolution are quantified on the following basis.

The first function considered is the two-dimensional wavenumber spectrum defined in equation (3.2.4) and computed as in equations (3.3.1) through (3.3.3) with the indicated restrictions. The resolution in and the reliability of this spectrum can be estimated from an analogy with time series analysis. Conventional definitions and arguments in the time and frequency domain are given in textbooks such as e.g. Bendat and Piersol (1971) or Jenkins and Watts (1968). One conventional definition of the frequency resolution is the width of the spectral window used in the computation of the frequency spectrum. When no tapering is used on the original data, the frequency window is the equivalent in the frequency domain of the function B_1 appearing in equation (3.3.7). This window is given below.

$$B_2(f) = \left\{\frac{\sin(\pi f T)}{f\pi}\right\}^2 \qquad (3.4.1)$$

However, a typical width parameter for such windows is not uniformly agreed upon in the literature, and another parameter may be used. It is the frequency interval between statistically independent estimates of the spectral density which for untapered data is equal to $1/T$ (Jenkins and Watts, 1968). These estimates are located at the points where $B_2(f)$ is zero.

all stereo photo pairs were oriented in exactly the same direction. In fact, this orientation is a random variable due to helicopter yaw during the photographic operation. This results in an increase of the region of resolution depending on the value of k (rotation around $\vec{k}=\vec{0}$). This increase is quantified in the discussion of the resolution of $\tilde{E}(k,\theta)$.

The reliability of the estimate $\tilde{E}(\vec{k})$ can be expressed in terms of its marginal probability density function, which is a χ^2-type distribution with the average equal to the expected value of the spectral estimate, and the number of degrees of freedom depending on the number of "raw" spectra used in the approximation of the ensemble average of equation (3.3.1). For one "raw" spectrum the number of degrees of freedom is 2 (Bendat and Piersol, 1971). Since N independent "raw" spectra were used, the total number of degrees of freedom (N_1) for the final estimate of $\tilde{E}(\vec{k})$ is 2N.

The second function which should be considered is the observed directional distribution $\tilde{D}(\theta,k)$. But the two-dimensional spectrum $\tilde{E}(k,\theta)$ should be considered first as it is an intermediate in the analysis. As indicated before, it was determined through interpolation in the two-dimensional wavenumber spectrum $\tilde{E}(\vec{k})$. The resolution of $\tilde{E}(k,\theta)$ can therefore be estimated from the resolution in $\tilde{E}(\vec{k})$. From the above arguments related to the statistical independence of the estimates of $E(\vec{k})$ in the $\vec{k}$-plane it appears that the resolution of $E(\vec{k})$ is equal to the mesh-size of the grid at which this spectrum was determined. This grid can be projected into the k,θ-plane where it produces a distorted rhombic pattern (fig. 3.4.2).

oriented in exactly the same direction. The directional bandwidth to be added will be on the order of twice the standard deviation of the helicopter yaw ($\sigma_{yaw} \simeq 0.06$, paragraph 2.2.3). The final expression for the directional resolution is given as

$$r_\theta \simeq \frac{\Delta k}{k} + 2\sigma_{yaw} \qquad (3.4.6)$$

The distance between the gridlines of the grid projected into the (k,θ)-plane in k-direction for a given value of θ (fig. 3.4.2) varies with θ from Δk_x to $\Delta k_x\sqrt{2}$. This indicates that the resolution along the k-axis (r_k) is approximately equal to $\Delta k_x = \Delta k_y$,

$$r_k \simeq \Delta k_x = \Delta k_y \qquad (3.4.7)$$

The reliability of the estimate $\tilde{E}(k,\theta)$ can be expressed in terms of a χ^2-distribution but the number of degrees of freedom (N_2) is not uniformly distributed over the (k,θ)-plane. It consitutes an undulating function due to the fact that the estimated value of $\tilde{E}(k,\theta)$ is based on the interpolation of four values of $E(\vec{k})$. The upper extreme of the undulating function occurs when a gridpoint in the k,θ-plane corresponds to the centre of a mesh of the regular grid in the $\vec{k}$-domain. The four values of $\tilde{E}(\vec{k})$ are then equally weighted in the determination of $\tilde{E}(k,\theta)$ and the number of degrees of freedom of each individual estimate of $\tilde{E}(k,\theta)$ is four times the degrees of freedom of each individual estimate of $\tilde{E}(\vec{k})$. The lower extreme occurs when the projected gridpoint (k,θ) coincides with a gridpoint of the regular $\vec{k}$-grid. In that case the number of degrees of freedom for $\tilde{E}(k,\theta)$ is equal to that for $\tilde{E}(\vec{k})$. The values of the two extremes are 8N and 2N.

The estimate of the directional distribution $\tilde{D}(\theta;k)$ is based on the evaluation of equation (3.3.21), from which it follows that the di-

The reliability of $\tilde{E}(f)$ can be estimated by counting the number of grid-points of $\tilde{E}(\vec{k})$ involved in the interpolation used to determine $\tilde{E}(f)$. This number is approximately the number of gridpoints of $\tilde{E}(\vec{k})$ on two circles with radii $k-\frac{1}{2}\Delta k$ and $k + \frac{1}{2}\Delta k$ in the $\vec{k}$-plane, with k corresponding to f. Half of the estimates of $\tilde{E}(\vec{k})$ on these circles are identical to the other half due to the 180^{0} ambiguity of $\tilde{E}(\vec{k})$. Consequently only half the number of estimates may be considered when determining the number of degrees of freedom of $\tilde{E}(f)$. As the number of degrees of freedom is 2N for each gridpoint of $\tilde{E}(\vec{k})$ it follows that the total number of degrees of freedom for $\tilde{E}(f)$, N_3, is given in the next equation.

$$N_3 = \frac{8\ \pi^2\ f^2}{g} \frac{N}{\Delta k} \qquad (3.4.11)$$

The estimation of the model parameters from the observations and the goodness-of-fit between the model and the observations will be addressed in the next paragraph.

3.5 Shape analysis

3.5.1 Introduction

The observations of the directional distributions obtained with the analysis described in the preceding paragraphs are relatively detailed. This detailed information is to be reduced to a manageable number of meaningful parameters to arrive at results which can be used for engineering or scientific purposes. Two methods are available to achieve this reduction. The first is based on assuming a model for the observed directional energy distributions. The parameters of such a model can be determined by fitting the model to the observations. It is important for the interpretations of these values to have a quantitative measure of the goodness-of-fit between model and observation. The second approach to reduce the detailed information is based on distribution-free parameters

In the least-squares method the difference V_1, defined below, is minimized while varying the width parameter s and the main direction $\overline{\theta}$ simultaneously.

$$V_1 = \sum_{i=1}^{M_1} [\tilde{D}(\theta_i) - \hat{D}(\theta_i)]^2 \qquad (3.5.1)$$

where θ_i is the discrete value of θ where the observation is available, and M_1 is their total number. $\tilde{D}(\theta)$ is the observed directional distribution and $\hat{D}(\theta)$ is the $\cos^{2s}(\theta/2)$-model with proper allowance for the 180^o ambiguity discussed in paragraph 3.2:

$$\hat{D}(\theta) = A\{\cos^{2s}(\frac{\theta - \overline{\theta}}{2}) + \cos^{2s}(\frac{\theta - \overline{\theta} + \pi}{2})\} \qquad (3.5.2)$$

A is a coefficient defined such that the integral of $\hat{D}(\theta)$ over the directional range from $-\pi$ to $+\pi$ is equal to one. Its value is

$$A = \frac{1}{4\sqrt{\pi}} \frac{\Gamma(s+1)}{\Gamma(s+\frac{1}{2})} \qquad (3.5.3)$$

A description of the actual numerical fit procedure is given in Appendix II.

The least-squares fit is applied only to those observed directional distributions which are considered to represent locally generated waves. This selection is described in paragraph 4.6.

3.5.3 Goodness-of-fit between model and observation

The $\cos^{2s}(\theta/2)$-model can be compared with each of the observed distributions individually. Several dozen of such distrubutions are available in this study and this would imply an equal number of comparisons. Some of these comparisons will be more interesting than others. For instance, the directional distribution near the peak of the spectrum is usually the actual analysis, the definition is:

$$V_2 = \frac{\sum_{i=1}^{M} [\tilde{E}_i - \hat{E}_i]^2}{\sum_{i=1}^{M} \tilde{E}_i^2} \qquad (3.5.8)$$

where the summation is over all combinations of discrete values (M) of k and θ. This notation is shorter and more convenient than the one used in *equation* (3.5.4).

The relative quadratic residual V_2 provides a quantitative overall measure of the difference between observation and model. However, it does not indicate whether the differences are statistically significant or not. The inclusion of this statistical aspect requires the introduction of the concept of statistical consistency. This concept is addressed next.

In the determination of the model parameters and of the goodness-of-fit as described above, the observation $\tilde{E}(k,\theta)$ was not explicitly considered as a random variable. Yet, it should be. The observation is a sample from a population of all possible observations which can be obtained in identical situations as regards the geophysical conditions and the observation technique and analysis. The question which is addressed with the concept of consistency is basically: to what extent may observed differences between model and observation be due to sample variability in the observation?

The consistency will be defined in terms of differences between two-dimensional spectra. These differences need to be defined before the definition of consistency can be given. They are again (as above) quadatric residuals. The first difference which is required is that between the expected value of the above described population, denoted by $\langle\,\rangle$, and the model of the observation:

$$\underline{V}_4 = \frac{\sum_{i=1}^{M} [\tilde{E}_i - \underline{\tilde{E}}_i]^2}{\sum_{i=1}^{M} \tilde{E}_i^2} \qquad (3.5.13)$$

The model spectrum $\hat{E}(k,\theta)$ is now said to be consistent with the observation $\tilde{E}(k,\theta)$ at the α-level when V_3 is equal to the α-fractile point of $p(V_4)$, the probability density function of $\underline{V}_4$.

It follows from the definition of the consistency between model and observation that, in order to determine the level of consistency, the probability density function $p(V_4)$ has to be estimated. This is done here by using a Monte-Carlo technique based on the assumed statistics of the observed two-dimensional wavenumber spectrum $\tilde{E}(\vec{k})$. It was shown in paragraph 3.4 that the values of $\tilde{E}(\vec{k})$ at different gridpoints in the $\vec{k}$-plane are considered to be random samples from populations which are mutually independent. Each of these populations was assumed to have an expected value of $< E(\vec{k}) >$ and a χ^2-distribution with 2N degrees of freedom. The probability density function $p(V_4)$ is estimated by first drawing sample spectra at random from the same populations, with the expected value of the χ^2-distribution replaced by the observation $\tilde{E}(\vec{k})$. Each of these sample spectra is transformed to the (k,θ)-domain with the transformation procedures described in paragraph 3.3. Subsequently the relative quadratic residual $\underline{V}_4$ is determined for each sample spectrum. This provides a set of sample values of $\underline{V}_4$ which is used to approximate $p(V_4)$ in a histogram.

The set of sample spectra obtained to estimate $p(V_4)$ is also used to estimate the sample variability of the model parameters s and θ. For each of the sample spectra, the values of s and θ are determined as a function of wavenumber k. The procedure described in paragraph 3.5.2 is used for this. The result is a set of samples of s and θ, for each discrete value of k. The sample variability of s is subsequently quantified with its standard deviation as a function of k. This information will be

It gives, in terms of the directional distributions, a weighted average of the relative area of difference between the observations and the model.

The description of the methods of observation and analysis which are used in this study is concluded here. The following chapter will review the actual observations of this study and the results of the analysis.

4.2 Geophysical conditions

4.2.1 Introduction

To obtain systematic dependencies between the directional wave parameters and other geophysical parameters, the two-dimensional wavenumber spectra were observed in a number of situations. The most basic one was called the ideal situation in paragraph 1.2. It was described as a situation with a homogeneous, stationary wind blowing perpendicularly off a straight coast over relatively deep water. These conditions were fairly well met during three observations off the coast of Holland. The parameter relationships found in these observations are tested for less ideal conditions by analyzing two more observations. The first of the observations was carried out off the coast of Holland in ideal conditions except that the wind was slanting across the coastline. The second of these observations was carried out in the German Bight near an irregular coastline in otherwise ideal geophysical conditions. These five observations concerned wavefields which were being generated by the local wind. A brief preview of the geophysical characteristics of the observations and a label number is given in tabel 4.2.1.

observation number	site	distance off-shore (km)	wind direction, wind speed (m/s)	coast
1	Noordwijk*	10	perpendicular off-shore, 6.0	long straight
2	Noordwijk	20	perpendicular off-shore, 6.0	long straight
3	Noordwijk	30	perpendicular off-shore, 6.0	long straight
4	Noordwijk	16.5	slanting off-shore, 10.0	long straight
5	Sylt**	46.2	perpendicular off-shore, 13.0	irregular

Table 4.2.1. Geophysical characteristics of the observations.
** = Holland, **= Germany.*

seen from the sea) over a distance which is long compared to the distance off-shore of the observations. These distances were 10, 16.5, 30 and 50 km. The general topography is indicated in the illustrations of the next paragraph. The German site is located off the island of Sylt. The bottom profile perpendicular to the coast of Sylt is very similar to the one at the Dutch site and this area can also be considered as deep water for waves generated by off-shore winds. During the preparation and execution of the field program it was assumed that the sector of the coast most relevant for the observation would be the coast of Sylt. This coast is rather smooth and slightly convex (as seen from the sea). However, it is found from the results of the observations that the coast line has to be considered on a larger scale. On this scale (150 km north-south, say) the coast is irregular. It is a tidal area with small islands and a large estuary to the south of the site of observation. The irregularity which is relevant is not so much due to the islands as well to the large indentation of the estuary. This is shown in the illustrations of the next paragraph 4.2.3. The distance off-shore (from Sylt) for the one observation at this site is 46.2 km.

4.2.3 Meteorological conditions

Three observations were carried out in a situation which came close to the ideal situation. These observations were carried out at the Noordwijk site on November 12th, 1976 at approximately 12.00 GMT. Synoptical information, provided by the Royal Netherlands Meteorological Institute, indicates that the wind field was dominated by three high pressure areas over Europe with rather low gradients of the pressure. This resulted in weak and variable winds on the scale of Europe. However, on the scale relevant to the observations the wind-field is judged to be sufficiently homogeneous and stationary to label the situation as an ideal situation. The wind speed was approximately

The wind speed in the southern North Sea varied from 3 to 12 m/s, but in the area relevant to the observation the wind field is again judged to be fairly homogeneous and stationary. The wind speed there was approximately 10 m/s and the wind direction was approximately 70° (nautical convention), which is approximately 50° backed with respect to the ideal off-shore direction. This situation is illustrated in fig. 4.2.3.

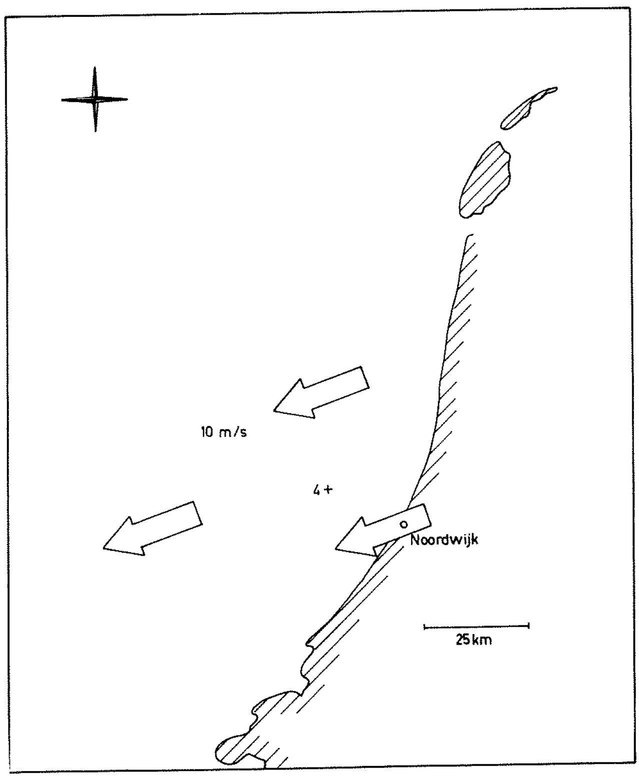

Fig. 4.2.3. Overall situation for observation 4.

The fifth observation was obtained off Sylt, again in a fairly homogeneous and stationary wind field. The weather was dominated by an atmospheric depression approaching the area of observation from the west.

4.3 Stereophotographic observations

The basic procedures which have been used to obtain the photogrammetric results have been described in paragraph 2.2. It will suffice here to indicate only the characteristics of the observations in terms of the variables of the photographic operations and of the photogrammetric analysis. These characteristics are given in Table 4.3.1, where the observations have been labeled by site and by observation number. The exact time of the observations is also given.

Two observations need a further qualification which follows below.

Observation number 1. Two areas of analysis are obtained from one stereo photo pair. These areas overlapped 40% in area.

Observation number 3. The eight areas of analysis are obtained from five stereo pairs. The photogrammetric analysis was such that from each of three pairs, two (overlapping) areas were obtained. The overlaps in area were 80%, 70% and 57%.

The influence of the overlapping of the areas on the spectral estimates is addressed in Appendix IV.

The exact numerical results of the photogrammetrical analysis do not seem to be relevant here. As an illustration a contourline map of one of the analyzed areas is shown in fig. 4.3.1.

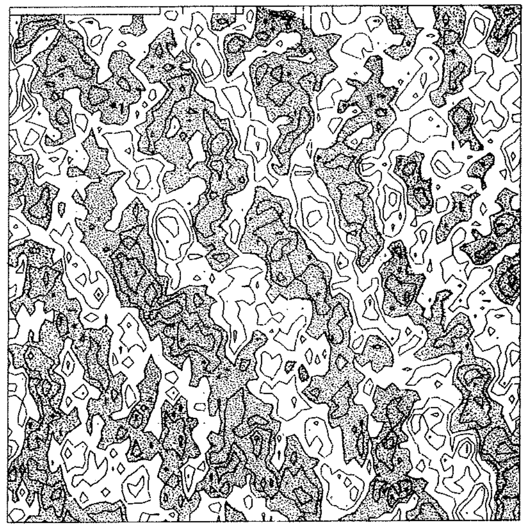

Fig. 4.3.1. Contourline plot of sea surface from observation 4. Contourline interval = 0.20 m, area = 170.0 x 170.0 m^2, shaded areas below mean sea level.

4.4 Wavenumber spectra

The results of the spectral analysis of the observations are presented in the form of contour line plots of the two-dimensional spectra, fig. 4.4.1 through 4.4.6. The resolution in the spectra is the reciprocal of the area sizes of table 4.3.1*. The contourlines seem to show a very detailed structure of these spectra but these details are mostly apparent because they are partly due to statistical variability. This variability is not very relevant for an interpretation in physical terms and smoothed versions of these illustrations are provided in paragraph 5.2. The Nyquist wavenumbers in x- and y-directions are the reciprocals of the mesh-size (which are also given in table 4.3.1) divided by two. The reliability is expressed in terms of the number of degrees of freedom of the χ^2-distribution in table 4.4.1. The peak wavenumbers of the spectra**, the directional resolution at this peak wavenumber and at twice this peak wavenumber are also given in this table.

* except for observation number 3, Appendix IV

** peak wavenumber of locally generated windsea (paragraph 4.6).

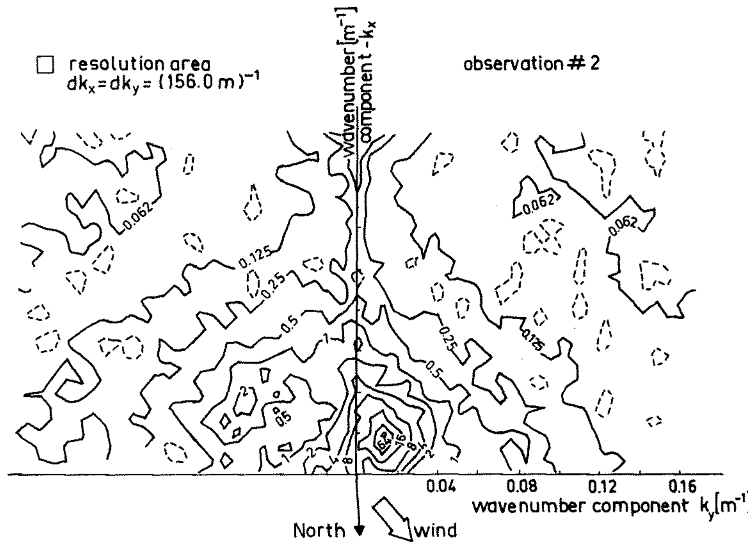

Fig. 4.4.2. Contourline plot of $\vec{k}$-spectrum of observation 2. Energy density in m^4. Minor variations are dashed.

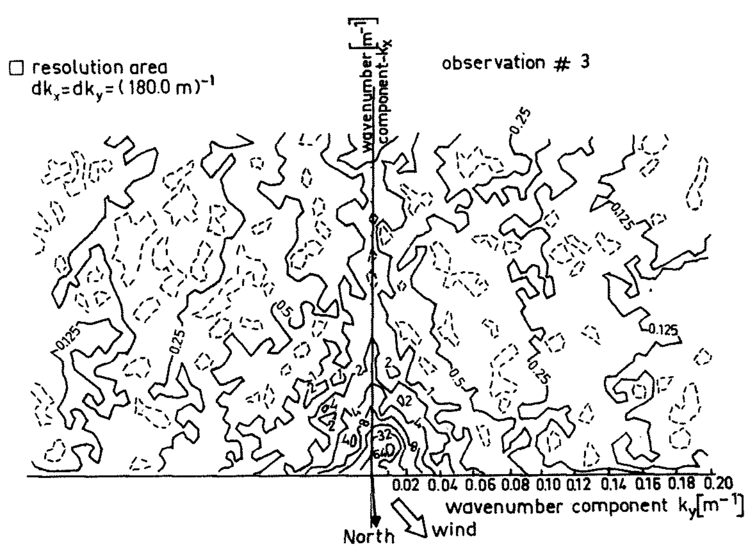

Fig. 4.4.3. Contourline plot of $\vec{k}$-spectrum of observation 3. Energy density in m^4. Minor variations are dashed.

4.5 Directional distributions

Only the most characteristic directional distributions are shown here. They were taken at the peak of the spectrum and at twice the peak wavenumber. These distributions are given in fig. 4.5.1. Illustrations of all directional distributions of observation 2, 4 and 5 are given in Holthuijsen (1978).

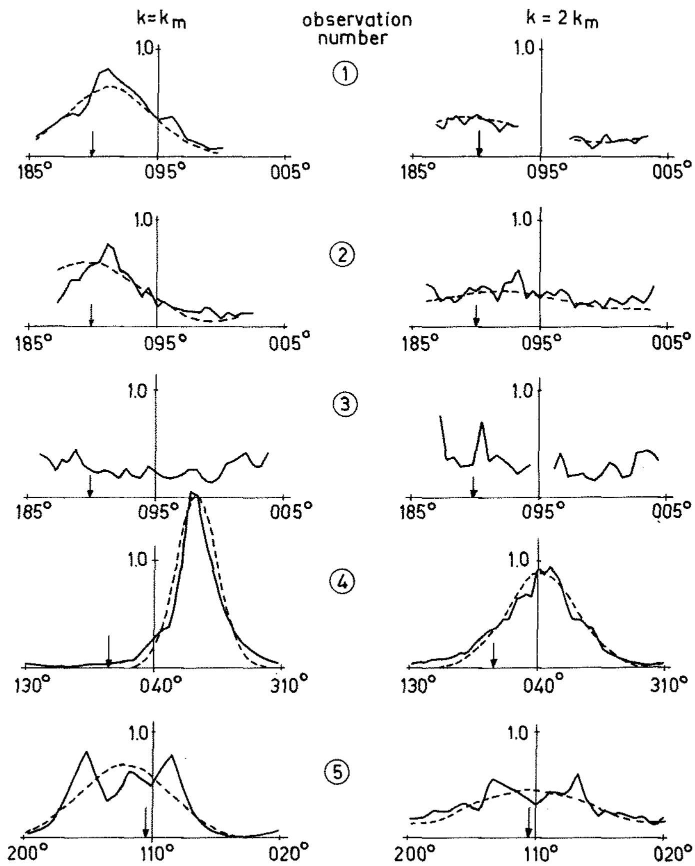

Fig. 4.5.1. Directional distributions at the peak wavenumber and at twice the peak wavenumber. Information in swell or noise area (paragraph 4.6) omitted. Arrows indicate wind direction. Dashed lines indicate best-fit model (paragraph 4.6).

The second aspect considered is the presence of swell. The spectra of observations 1,2 and 3 (figs. 4.4.1, 4.4.2 and 4.4.3) seem each to be composed of two spectra: one corresponding to the locally generated sea with the peak in the direction of the local wind and one corresponding to wavecomponents probably generated in an area south-west of the area of observation (direction 220°). This aspect of the observations is discussed more in detail in paragraph 5.2 where this second wave field is conveniently characterized as swell. The plots of the smoothed contourlines presented in that paragraph facilitate the reading of the illustrations just mentioned.

In the spectra of observations 1 and 2 the difference in location of the peaks of the swell and the locally generated sea seem sufficiently large to separate the two spectra but the identification of the swell-region in these spectra is still rather subjective. Describing the topography of the spectrum as two peaks with a valley in between, the line separating the locally generated sea from the swell is taken to be the bottom line of the valley. At the sides of the swell peak not facing the peak of the locally generated sea the distinction is much more vague and the choice between swell and locally generated sea is rather arbitrary. The result of these subjective choices is also indicated in Appendix V.

The above procedure to identify the swell cannot be used in the spectrum of observation 3 because the sea and swell spectra overlap considerably. This is commented upon in the next chapter. In view of this overlap, and in part also because of the poor reliability of the observation, this spectrum is excluded from further analysis.

The spectra, cleansed from noise and swell, is further investigated to determine the directional characteristics. The information in the spectra in the areas identified above was ignored. Thus, the $\cos^{2s}(\theta/2)$-model of equation (3.5.2) is fitted to the observed spectra only for the regions

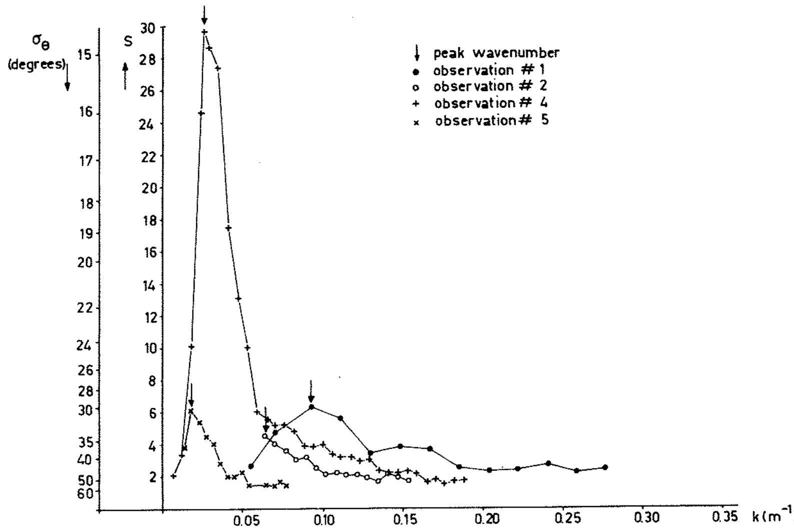

Fig. 4.6.2. Directional width parameter s as function of wavenumber. Swell and noise omitted.

To illustrate the directional width in terms of a directional sector, the standard deviation of the $\cos^{2s}(\theta/2)$-model of equation 1.2.3 is also plotted along the s-axis. This standard deviation σ_θ is defined as

$$\sigma_\theta = \int_{-\pi}^{+\pi} \theta^2 \cos^{2s}(\theta/2)\,d\theta \qquad (4.6.1)$$

This integral was numerically evaluated for s = 1 to 100 ($8^\circ < \sigma_\theta < 65^\circ$) and the results were approximated with

$$\sigma_\theta \simeq 65 s^{-0.43} \quad \text{(degrees)} \qquad (4.6.2)$$

The error of this approximation is less than 1.5° for $8^\circ < \sigma_\theta < 30^\circ$ and less than 2.5° for $30^\circ < \sigma_\theta < 65^\circ$.

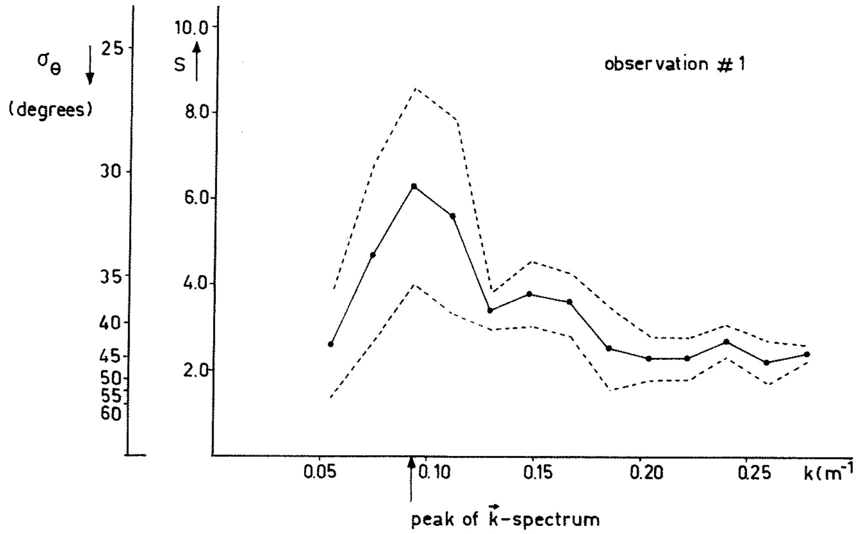

Fig. 4.6.4. Variability of directional width parameter s in observation 1. Dashed lines indicate observed value + or − one standard deviation.

4.7 Goodness-of-fit between model and observation

The difference between each observed spectrum and its best-fit model has been quantified in the residuals $V_2^{\frac{1}{2}}$ (the normalized standard deviation) and V_5 (the normalized absolute difference), as described in paragraph 3.5.3. When determining these residuals, the noise and swell regions in the observed spectra are again ignored by excluding these regions from the summations in equations (3.5.8 and 3.5.15). The results are listed in table (4.7.1). A visual appreciation of the difference between observation and model can be obtained from fig. 4.5.1, while a brief discussion of these differences is provided in paragraph 5.2.

4.8 Frequency spectra

The frequency spectra of the observed waves are determined in two ways. The first is to transform the two-dimensional wavenumber spectrum which was obtained through the stereophotogrammetric operations, paragraph 3.3. The second way is to analyze time series of sea surface elevations as described in Appendix VII. The sole purpose of determining the frequency spectra is to have an intercomparison. It is obviously necessary for such a comparison that the stereophotographic observation and the time series are obtained at the same location and at the same time. Unfortunately such coincidence in time and space was achieved only for observation number 2 (the ideal situation) and for a testcase. For observation number 5 (the irregular coast situation) simultaneous observations at sea level were only available at locations other than the one of the stereophotographic observation. These observations at sea level could be hindcasted fairly well with a simple method. This method was used with the same geophysical information to hindcast the frequency spectrum at the location of the stereophotographic observation.

The observations in the testcase requires some comment as it was almost completely ignored in the preceding text. It was obtained during a flight to test the equipment and operational procedures where little attention was paid to an optimal altitude of photography. As it happens to be one of the three situations which was analyzed and where groundtruth is available, it is included here. The geophysical situation during this flight was not interesting from a scientific point of view and it was therefore ignored sofar. Information on this testcase is provided in Appendix VIII.

A detailed description of the above frequency spectra is not given here as it would distract too much from the current text. The main results are

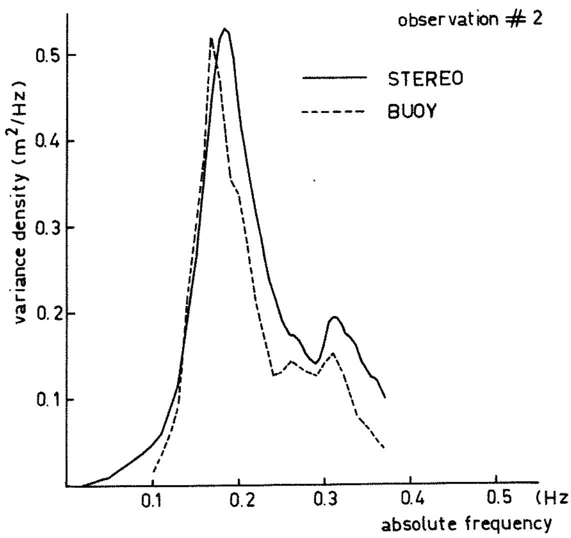

Fig. 4.8.1. Frequency spectra observation 2.

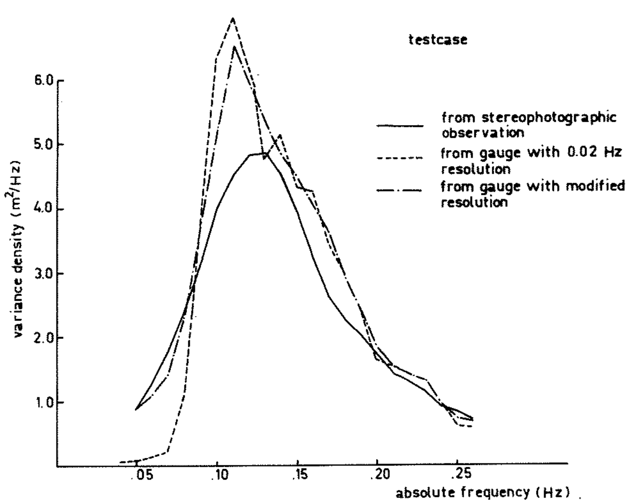

Fig. 4.8.2. Frequency spectra testcase.

5. Discussion

5.1 Introduction

The discussion of the results will pertain mainly to three aspects of the observations. The first concerns the influence of the upwind coastline on the shape of the observed directional distributions. It will be discussed in terms of directionally decoupled wave generation. The second aspect is the correspondence of the observed directional energy distributions with the selected $\cos^{2s}(\theta/2)$-model. The third aspect concerns the relationship between the directional width parameter s and relevant geophysical parameters.

5.2 General discussion

The illustrations of the observed two-dimensional wavenumber spectra as presented in paragraph 4.4 show rather fine details. These details are to some degree due to the statistical variablility of the observations which are not relevant for an interpretation in physical terms. To facilitate the discussion of these spectra other illustrations are presented which were drawn rather subjectively as a kind of smoothed versions of the contourline plots of paragraph 4.4. This was done such that the most significant shape-aspects of the spectra are emphasized. They do not represent the result of a formal operation.

The ideal situation (observations 1, 2 and 3)

Smoothed contourline plots of the two-dimensional spectra of the first three observations (the ideal situation, off the Dutch coast, figs. 4.4.1 through 4.4.3) are given in fig. 5.2.1.

direction, not so well defined since it is much broader and with secondary maxima.

The sharp peak at approximately 220^o represents waves which were probably generated in an area somewhere to the south-west of the area of observation. However, it is not possible with stereophotography to discriminate wavecomponents traveling in opposite directions so that from these spectra alone one may as well conclude that these waves were generated in an area to the north-east of the area of observation. This was physically possible since both directions (220^o and 40^o) are almost parallel to the coast. But a close inspection of detailed weather maps at the Royal Netherlands Meteorological Institute suggested that these wave-components were generated near the Strait of Dover (230^o from the area of observation). They are considered to be swell.

The two peaks in each of the spectra of observation numbers 1 and 2 (10 and 30 km off-shore respectively) are well separated, both in direction and scalar wavenumber. It was possible, as noted in paragraph 4.6, to identify the directional characteristics of the locally generated waves independently (or almost independently) from those of the swell. In observation number 3 (50 km off-shore) the two peaks seem to be also well separated but the spectrum of the locally generated waves could not be distinguished from the spectrum of the swell as it was poorly defined. This poor definition of the locally generated spectrum caused this spectrum to be dropped from further consideration.

A visual inspection of the contourlines of the spectra which were generated in the ideal situation does not readily reveal similarities in shape or other systematic dependencies. A visual inspection of the observed directional distribution functions (e.g. fig. 4.5.1) is slightly more instructive. From the spectra of observations numbered 1 and 2 it appears that these functions are essentially uni-modal for the

This spectrum has one rather pronounced peak at approximately 15^{o}, that is a direction more or less parallel to the coast. This is, at first sight, a surprising observation since the wind was blowing across the coastline. The locally generated wavecomponents at the peak (those coming more or less from the local wind direction) are dominated by wavecomponents coming from the north. This dominance disappears for higher wavenumbers where the main direction of the spectrum is aligned more closely with the wind direction. As in observation 1 and 2, it appears that the directional distribution functions are essentially uni-modal and most narrow at the peak of the spectrum.

The fact that the wavecomponents from the north dominate the locally generated wavecomponents near the peak of the spectrum suggests directionally decoupled generation of the waves by the wind. This aspect of wave generation will be addressed separately in paragraph 5.3. The dominance of the waves from the north also points out that the windfield north of the area of observation is more relevant to the interpretation than the windfield to the south. This supports the interpretation of the windfield made in Appendix III.

The irregular coast situation

The smoothed contourlines of the spectrum of observation number 5, (the irregular coast situation, fig. 4.4.5) and the overall geophysical situation are given below.

rectionally decoupled generation of waves, the subject of the next paragraph.

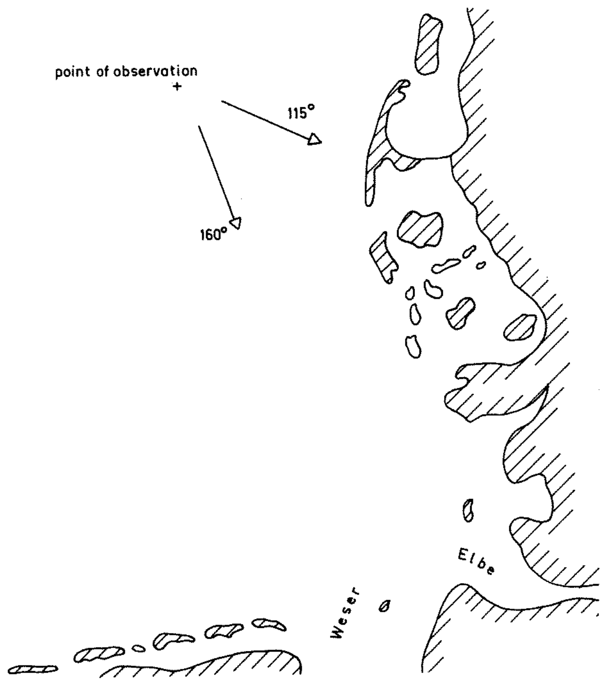

Fig. 5.2.4. Principal wave directions in observation 5.

The peak in the direction of the wind is bi-modal (fig. 4.4.5): two peaks could be identified differing approximately + 15^{o} and - 15^{o} in direction from the wind direction. This feature of the spectrum seems real in the sense that the directional resolution (21^{o} near this peak) and reliability (χ^2-distribution with 18 degrees of freedom) seems to be sufficient to distinguish these peaks statistically. This aspect of the observation is possibly related to physical processes such as for instance the nonlinear interactions computed by Fox (1976). The distribution of these interactions, into the forward direction from the peak (towards lower frequencies) is also bi-modal in shape. It is noted that also some of the observations of Tyler et al. (1974) showed bi-modality near the peak of the directional distributions. However, this current much stronger than estimated (2.2 m/s instead of the estimated 0.9 m/s) which does not seem to be realistic. Still, tidal information from tables and maps alone is possibly inadequate for the above comparison.

The frequency spectrum from the stereo pictures obtained in the test-case agrees fairly well with the spectrum obtained from the wave gauge for frequencies higher than f = 0.13 Hz, say (fig. 4.8.2). The discrepancy for lower frequencies was substantial.

The agreement in observation number 5 between the spectra obtained from the stereo data and from the hindcast is satisfactory considering the differences between observed and hindcasted spectra at the other locations (Appendix VII).

Conclusions

From a visual inspection of the observed directional distribution functions in the ideal situation and in the slanting wind situation it appears that these functions are essentially uni-modal and that they are most narrow near the peak of the spectrum. This is in agreement with observations of Tyler et al. (1974), Mitsuyasu et al. (1975) and Hasselmann et al. (1980).

The observed spectra in the slanting wind situation and in the irregular coast situation are strongly influenced by the geometry of the up-wind coastline. This suggests directionally decoupled generation of the waves.

The agreement between the frequency spectra obtained at sea level and from the stereo photos varies from poor to satisfactory. The source of characteristics of the wave spectrum one can hindcast wave components from different directions independently from each other. A model that can be used for such directionally decoupled hindcasts has been suggested by Seymour (1977). An essentially identical model has been used in this study. It is described next.

Consider a stationary,homogeneous windfield over a deep water basin with an arbitrary geometry of the coastline, fig. (5.3.1)

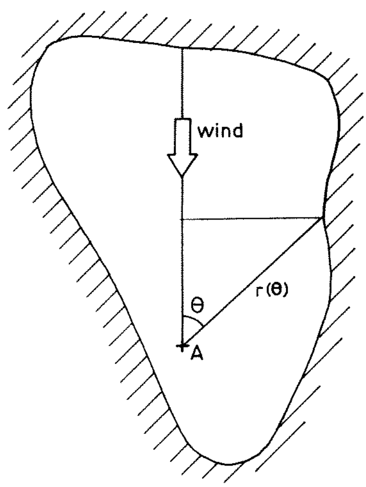

Fig. 5.3.1. Definitions for Seymour model.

The hindcast in a point A is first concentrated on wave components from an arbitrarily chosen direction θ. These components are assumed to be generated independently from components travelling in other directions. The only relevant independentvariables for these components are then, the direction relative to the wind direction (θ) and the distance to shore in that direction (r(θ)).The windspeed (U) and the gravitational acceleration (g) are also relevant parameters but they are constants parameters and to determine these parameters from established relationships with fetch and windspeed. The shape of the spectrum in the ideal situation is assumed to be that of the JONSWAP-spectrum (Hasselmann et al.,1973) with a $\cos^{2s}(\theta/2)$- directional distribution. The parameter relationships are taken from Günther et al. (1979) for the frequency spectrum and from Hasselmann et al. (1980) for the directional distribution function. However, these relationships have been slightly modified as described in Appendix IX.

The model is used to hindcast the spectra for the conditions of observations 4 and 5 which are the slanting wind situation and the irregular coast situation. Observation number 5 will be considered before observation number 4 because the situation of observation number 5 illustrates the above argument more clearly than does the other situation.

The spectrum observed through the stereophotographic technique in the situation with the irregular coast (observation 5) showed two major peaks: one peak at $f = 0.175$ Hz and $\theta = 160^{\circ}$ and a double peak at $f = 0.17$ Hz and $\theta \simeq 115^{\circ}$ (fig. 5.5.23 and 5.3.3). The direction of the double peak corresponded to the wind direction ($\theta = 115^{\circ}$) and the direction of the other peak corresponded to the area off the Weser- and Elbe-estuaries (fig. 5.2.4).

The hindcast of the spectrum in this situation (fig. 5.3.3 and Appendix X) contains also two peaks: one narrow peak at $f \simeq 0.16$ Hz and $\theta \simeq 150^{\circ}$ and one rather broad (directionally) peak at $f \simeq 0.20$ Hz and $\theta \simeq 120^{\circ}$.

The frequencies of the hindcasted peaks differ from the frequencies of the observed peaks but the directions of the hindcasted and observed peaks agree fairly well. The direction of the narrow peak hindcasted at

The above agreement in directional aspects between observation and hindcast suggests that the waves generated off Sylt did not interact appreciably with the waves generated in the area off the Weser-Elbe-estuaries. In other words, the nonlinear interactions were not strong enough (or, the dimensions of the generating area were too small) to force the two-dimensional spectrum into a standard shape at the point of observation.

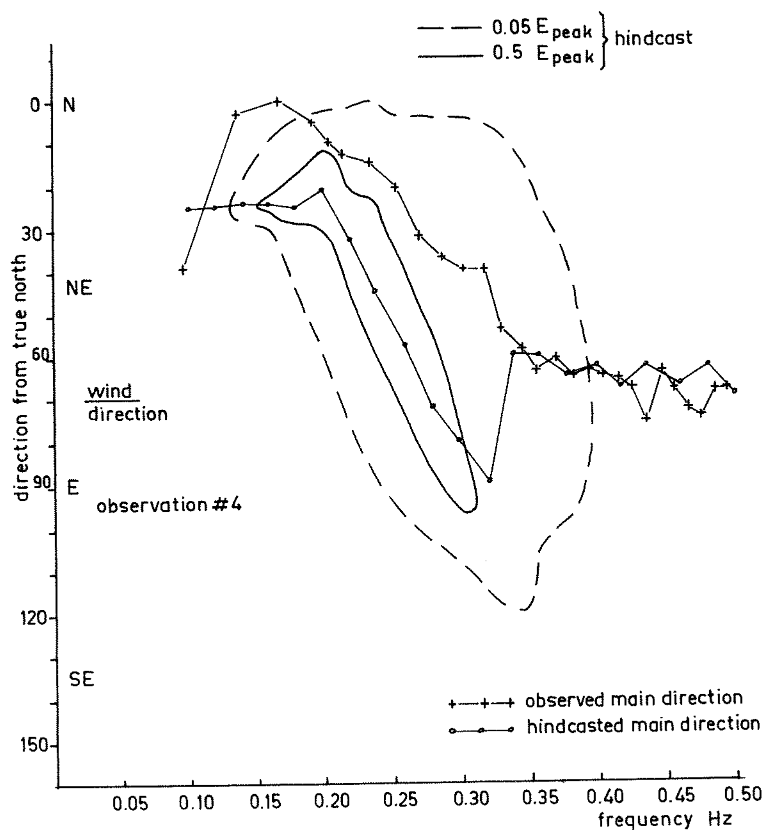

Fig. 5.3.4. Hindcasted and observed main direction as function of frequency for observation 4.

It was verified to be directly related to the overshoot of the frequency spectrum as a function of fetch (e.g. Hasselmann et al., 1973). For instance, the component f = 0.32 Hz from the wind direction + 30^{o} (southerly) is in the overshoot-phase of its development whereas the directionally "symmetric" component (f = 0.32 Hz from $\theta = \theta_{wind} - 30^{o}$) had already passed that phase.

Conclusion

The qualitative agreement between observed and hindcasted directional characteristics of the two-dimensional spectra in the slanting wind situation and in the irregular coast situation supports the suggestion of directionally decoupled wave generation.

5.4 The directional distribution

The difference between the observed directional distributions and the $\cos^{2s}(\theta/2)$-model can be quantified with the relative standard deviation $V_2^{\frac{1}{2}}$ and the relative absolute residual V_5. The values of these residuals as obtained from the observations in this study were listed in table 4.7.1. A visual impression of the differences between some characteristic observations and the model was provided in fig. 4.5.1. It is obvious that the best agreement between model and observation in terms of the absolute measure V_5, is obtained for observation 1 and 2 (ideal situation). The agreement is slightly poorer for observation 4 (slanting wind situation) and poorer still for observation 5 (irregular coast situation). The poor fit of the last observation is emphasized by the value of the relative standard deviation $V_2^{\frac{1}{2}}$.

The numerical values of the residuals $V_2^{\frac{1}{2}}$ and V_5 are difficult to interpret in an absolute sense because an appreciation of these numbers depends to a large extent on the purpose of modelling the spectrum.

in the histogram of fig. 4.6.5. It is found that the model is highly consistent ($\alpha = 0.79$) with the observation. In fact, the difference between model and observation (in terms of the relative quadratic residual) is almost equal to the most likely difference between this observation and a repeated observation (in an identical situation).

Conclusions

The observed values of the relative residuals indicate that the best agreement between the observed directional distributions and the $\cos^{2s}(\theta/2)$-model is found in the ideal situation. The agreement in the slanting wind situation is almost the same. The agreement in the irregular coast situation is considered to be poor.

The observed differences between model and observation in the ideal situation in this study are slightly greater than those reported in the literature for a few detailed observations in a slowwly varying wind-field . The discrepancy is partly due to the fact that the model used for these few observations had one more degree of freedom than the model used in this study. It may also be due to unknown differences in the sample variabilities of the observations.

The $\cos^{2s}(\theta/2)$-model is a realistic model for observation number 1 (ideal situation) as the model and the observation were statistically consistent at the high level of $\alpha = 0.79$.

5.5 The directional width

The values of the directional width parameter s observed in this study will be compared here with the suggestions of Mitsuyasu et al. (1975) and Hasselmann et al. (1980). The suggestions will be presented and commented upon before making the comparison.

spectrum (s_m):

$$\tilde{s} = \frac{s}{s_m} \tag{5.5.5}$$

With the above transformations, the expressions of Mitsuyasu et al. (1975) can be written as

$$\left.\begin{aligned} \tilde{s} &= \tilde{k}^{2.5} && \text{for} \quad \tilde{k} < 1 \\ \tilde{s} &= \tilde{k}^{-1.25} && \text{for} \quad \tilde{k} \geqslant 1 \end{aligned}\right\} \tag{5.5.5}$$

with $$s_m = 11.5\ \beta^{2.5} \tag{5.5.6}$$

The expressions due to Hasselmann et al. (1980) are,

$$\left.\begin{aligned} \tilde{s} &= \tilde{k}^{2.03} && \text{for} \quad \tilde{k} < 1 \\ \tilde{s} &= \tilde{k}^{(-0.32\ -\ 0.72\ \beta^{-1})} && \text{for} \quad \tilde{k} \geqslant 1 \end{aligned}\right\} \tag{5.5.7}$$

with $$\left.\begin{aligned} s_m &= 6.97 && \text{for} \quad k < 1 \\ s_m &= 9.77 && \text{for} \quad k \geqslant 1 \end{aligned}\right\} \tag{5.5.8}$$

It appears from the above expressions that Hasselmann et al. (1980) found that the function $\tilde{s}(\tilde{k})$ depends on the wave age β with s_m a constant. Mitsuyasu et al. (1975) found the reverse to be true. These differences may be due to differences in the observations which were used to determine the above suggestions. The comments given next will indicate some of these differences.

The suggestions of Mitsuyasu et al. (1975) are to be used for the "idealized" spectrum according to these authors. This is taken to is academic in that the effect of this averaging is negligible was not investigated here, but the peakedness of the relationship between s and the frequency suggests that it is not.

To evaluate the differences between the data of this study and the above empirical information, it is appropriate to consider the statistical variation of the data of this study and of the data of Hasselmann et al. (1980). The standard deviation of s (σ_s, fig. 4.6.4) for observation 1 may be roughly estimated as

$$\sigma_s \simeq 0.3 \ s \qquad (5.5.9)$$

This expression will be used further to estimate the standard deviation of all observations of this study. The variation in the data of Hasselmann et al. (1980) can only be indicated with the ranges of observed values of s and β as determined from their publication.

The data of Mitsuyasu et al. (1975) are not compared with the observations of the present study whereas their analytical expressions are. The reason for not comparing the data is that the difference between the two data sets in terms of observed values of β is too great to make a meaningful comparison. The analytical expressions, on the other hand, are suggested to be applicable on a wider range of β values than originally observed. A comparison with the data of the present study is therefore useful.

The function $s_m(\beta)$

The values of s_m observed in this study as a function of the wave age β are plotted in fig. 5.5.1 with the suggestions of Mitsuyasu et al. (1975) and Hasselmann et al. (1980). To illustrate the width of the observed directional distribution in terms of a directional sector, crepancy between the observations and the $\cos^{2s}(\theta/2)$-model is less than in observation 5 but where the directional distribution function is apparently much more narrow (s much larger) than one would expect from the data of Hasselmann et al. (1980).

As for the agreement between the suggestions of Hasselmann et al. (1980) and Mitsuyasu et al. (1975) on the one hand, and the data of this study on the other, observations 1 and 5 agree well with these suggestions, the difference being approximately equal to the estimated standard deviation. It is not possible to determine a preference for either of the suggestions on the basis of these two data points because the differences are approximately equal for both suggestions and because the number of data points is too small. Observation 2 and 4 do not agree well with the suggestions.

The function $\tilde{s}(\tilde{k})$

The observed normalized values of s ($\tilde{s} = s/s_m$) as a function of the normalized wavenumber ($\tilde{k} = k/k_m$) are plotted in figs. 5.5.2 through 5.5.5 along with the suggestions of Mitsuyasu et al. (1975) and Hasselmann et al. (1980). The most obvious qualitative agreement between the data of this study and the suggestions is that s is at its maximum at $k=k_m$ ($\tilde{s}=1$) and that $\tilde{s}$ decreases as the wavenumber decreases or increases from $k=k_m$. The quantitative evaluation will be presented next for $\tilde{k}<1$ and $\tilde{k}>1$ separately.

The few observations of this study for $\tilde{k}<1$ agree well with both suggestions (fig. 5.5.2, 5.5.4 and 5.5.5) as the differences are typically less than the estimated standard deviation of the observed value of $\tilde{s}$ (equal to the standard deviation of s, equation 5.5.9, for a constant value of s_m).

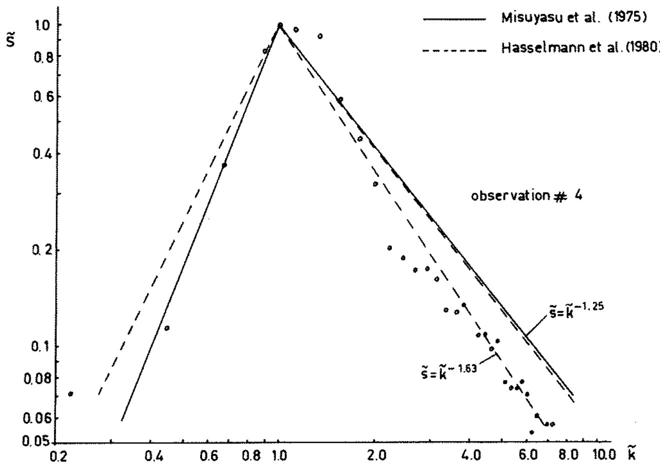

Fig. 5.5.4. The normalized directional width parameter $\tilde{s}$ *as a function of the normalized wavenumber* $\tilde{k}$, *observation 4.*

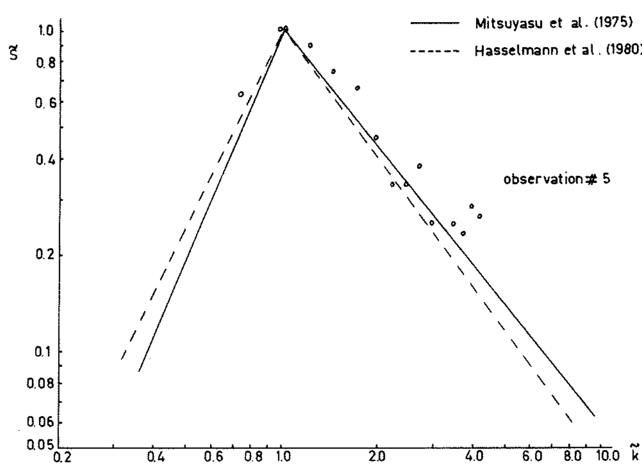

Fig. 5.5.5. The normalized directional width parameter $\tilde{s}$ *as a function of the normalized wavenumber* $\tilde{k}$, *observation 5.*

The value of s at the peak of the spectrum is found to be the maximum value of s in each of the observed spectra. This is in agreement with the observations and suggestions of Mitsuyasu et al. (1975) and Hasselmann et al. (1980).

The observed normalized values of s ($\tilde{s} = s/s_m$) as a function of the normalized wavenumber ($\tilde{k} = k/k_m$ where k_m is the wavenumber at the peak of the spectrum), again excluding the observations in the slanting wind situation, are on the average slightly higher (by approximately 20%) than the suggestions of Mitsuyasu et al. (1975) and Hasselmann et al. (1980). The observed dependency of $\tilde{s}$ on $\tilde{k}$ in the slanting wind situation is similar in shape to the suggestions but the decrease of $\tilde{s}$ for increasing values of $\tilde{k}$ is more rapid in the observations than it is in these suggestions.

may therefore indicate a limitation to the assumed influence of nonlinear wave-wave interactions on which advanced wave prediction models are based. It follows that wave prediction for most inland waters (being on the scale of dozens of kilometers) should be based on directionally decoupled models rather than models in which a standard spectrum is assumed.

The shape of the directional distribution functions observed in the ideal situation was quantitatively compared with the $\cos^{2s}(\theta/2)$-model. The differences are acceptable for most practical purposes. In fact, the differences which are found may not be statistically significant because a quantitative assessment of the sample variability of one of the observed spectra indicates that for this spectrum the observations and the $\cos^{2s}(\theta/2)$-model are statistically consistent at a high level.

The $\cos^{2s}(\theta/2)$-model fits also relatively well to the observations in the slanting wind situation, but the main direction of the wave energy (as a function of frequency) differs considerably from the wind direction. This discrepancy could be attributed, at least qualitatively, to directionally decoupled wave generation as discussed above. A similar conclusion is drawn from the observations in the irregular coast situation where no acceptable agreement is found between observations and the $\cos^{2s}(\theta/2)$-model.

Empirical relationships between the width parameter s of the $\cos^{2s}(\theta/2)$-model on the one side and the frequency and the windspeed on the other have been suggested by Mitsuyasu et al. (1975) and Hasselmann et al. (1980). The differences between these suggestions are considerable and preference should be given to the suggestions of Hasselmann et al. (1980) because their data are quantitatively and qualitatively superior to those of Mitsuyasu et al. (1975). The observations of the present study

Empirical information can also be used to determine certain aspects of the assumed universal shape of the two-dimensional spectrum. For instance, the universal relationship between the directional width as a function of frequency and windspeed as suggested by Hasselmann et al. (1980) needs a broader empirical basis because the scatter in the original data is unacceptably large. Routine single-point observations such as e.g. with a pitch-and-roll buoy may be very useful in this. These goals are relatively short-term objectives for the research of ocean wave directionality. Long-term objectives may include establishing the limitations of the applicability of the assumed universal two-dimensional spectrum. These limitations are closely related to the response of non-linear wave-wave interactions to variations in the windfield. Theoretical models for this response should be developed and the results should be compared with observations in the oceanic environment.

of the Royal Netherlands Meteorological Institute for his support, his interest and his helpful suggestions.

Thanks is due to the people at the Royal Netherlands Meteorological Institute and the Institute of Applied Physics who provided me with meteorological and oceanographical data during the field operations off the coast of Holland.

It may be inferred from the description in this thesis that the number of individuals contributing directly to the study has been large (probably a few dozen). I would like to thank each one of them but I can mention only a few. The electronic equipment was designed and built by mr. G.W. Lubking and mr. G.J. v.d. Vliet. I am particularly grateful to mr. v.d. Vliet because he also endured some very frustrating field operations. I would like to extend the same thanks to the photographer mr. N.F.M. Bergen-Henegouwen and his assistants, not only for their efforts during the preparation and execution of the photographic missions but also for their meticulous handling of the films. The laborious and tedious work of analyzing the stereophotographs was carried out by miss J. Kronenberg and her colleagues. I am very well aware that their work has been relatively unrewarding, analyzing dozens of dull pictures of the sea surface. Their work has been most important and I am very grateful to them.

I am also grateful to mrs. C.M. Muilman and miss M.J. v.d. Brugge for typing the draft. Fortunately they could read my handwriting. Mr. W.F.H. Ritter and mr. J.W. Muilman made the drawings. Their accurate and speedy work is most appreciated.

List of symbols

Most of the symbols used in the text are listed below. Symbols which have been used only locally have not been listed. The arguments of functions have not been indicated here. The context in which functions are used provides a more specific meaning of the function symbol.

A	normalization coefficient of model energy distribution
b	distance between cameras
$b_1(\ )$	two-dimensional box-car function
$B_1(\ )$	spectrum of box-car function $b_1(\ )$
$B_2(\ )$	spectrum of one-dimensional box-car function
c	phase speed
c_m	phase speed at peak frequency f_m
c_g	velocity of energy propagation
$C(\ )$	covariance function of sea surface elevation
d	water depth
$D(\ )$	directional energy distribution without 180^0 discriminatioı
$D_o(\ )$	directional energy distribution with 180^o discrimination
$\tilde{D}(\ )$	observed directional energy distribution
$\hat{D}(\ )$	model directional energy distribution
$E(\ )$	variance (energy) density spectrum
$E_o(\ )$	variance (energy) density spectrum
$\hat{E}(\ )$	variance (energy) density spectrum (model)
$\tilde{E}(\ )$	observed energy density spectrum, final estimate
f	frequency, focal length
f_m	peak frequency, frequency at peak of frequency spectrum
$\tilde{f}$	frequency normalized with peak frequency f_m
$\tilde{f}_m$	peak frequency normalized with windspeed and gravitational acceleration
$\hat{f}$	frequency normalized with windspeed and gravitational acceleration

$p(\ )$	probability density function
r	resolution bandwidth
$\vec{r}$	displacement vector
$\vec{R}$	spatial limit of integration in Fourier transformation
s	directional width parameter of $\cos^{2s}(\theta/2)$-model
s_m	value of s at peak of spectrum
t	time
T	length of wave record
U	average wind speed at 10 m elevation
U_z	average windspeed at elevation z meter
V	magnitude of mean current vector
$\vec{V}$	mean current vector
V_1	summed squared difference
V_i	$i>1$, relative residual between observation and model
x	horizontal coordinate, fetch in ideal generation situation
$\tilde{x}$	fetch x normalized with windspeed and gravitational accelleration
x_i	discrete value of horizontal coordinate x
$\vec{x}$	place vector
y	horizontal coordinate
y_i	discrete value of horizontal coordinate y
z	vertical coordinate
α	energy scale parameter of JONSWAP frequency spectrum
α_o	constant in model directional energy distribution
β	wave age, c_m/U
$\gamma(\ )$	peak enhancement function of JONSWAP frequency spectrum
γ_o	shape parameter of JONSWAP frequency spectrum
$\delta(\ )$	delta function
$\Delta(\ )$	set of delta functions
$\Delta^*(\ )$	spectrum of set of delta functions $\Delta(\ )$
$\varepsilon(\ )$	noise in stereophotogrammetric results

List of references

Anonymous (1972), *Tide tables for the seaports in the Netherlands and for Antwerp and Zeebrugge, 1973*, Directorate for Watermanagement and Hydraulic Research of Rijkswaterstaat, Staatsuitgeverij, 's-Gravenhage, Netherlands

Anonymous (1975), *Tide tables for the seaports in the Netherlands and for Antwerp and Zeebrugge*, Directorate for Watermanagement and Hydraulic Research of Rijkswaterstaat, Staatsuitgeverij, 's-Gravenhage, Netherlands

Anonymous (1976), *Stroomatlas, Noordzee, zuidelijk deel*, Ministerie van Defensie, Afdeling Hydrografie, 's-Gravenhage, Netherlands

Bendat, J.S. and A.G. Piersol (1971), *Random Data: Analysis and Measurement Procedures*, Wiley-Interscience, New York

Bouws, E. (1978), *Wind and wave climate in the Netherlands sector of the North Sea between 53^o and 54^o north latitude*, Koninklijk Nederlands Meteorologisch Instituut, de Bilt, Wetenschappelijk Rapport, W.R.78-9

Brnjac, M., L.J. Carlsen, R.G. McDonald and R. Orth (1976), *Digital terrain models from the Gestalt Photomapper II*, Gestalt International Limited, Vancouver, Canada

Brümmer, B., D. Heinricy, L. Krügermeyer and D. Prümm (1974), *The Large Scale Weather Features over the North Sea during the JONSWAP II Experiment*, Berichte des Instituts für Radiometeorologie und Maritieme Meteorologie, Universität Hamburg, Institut der Frauenhofer Gesellschaft, Nr. 24

Cooley, J.W. and J.W. Tukey (1967), *The Fast Fourier Transform*, IEEE Spectrum, Vol. 4, pp. 63-70

Cote, L.J., J.O. Davis, W. Marks, R.J. McGough, E. Mehr, W.J. Pierson, J.F. Ropek, G. Stephenson and R.C. Vetter (1960), *The directional spectrum of a wind generated sea as determined from data obtained* *wave spectrum, Part 2, Conservation theorems, wave-particle correspondence, irreversibility*, Journal of Fluid Mechanics, Vol. 15, No. 2, pp. 273-281

Hasselmann, K., R.P. Barnett, E. Bouws, H. Carlsen, D.E. Cartwright, K. Enke, J.A. Ewing, H. Gienapp, D.E. Hasselmann, P. Kruseman, A. Meerburg, P. Müller, D.J. Olbers, K. Richter, W. Sell and H. Walden (1973), *Measurements of Wind-Wave Growth and Swell Decay during the Joint North Sea Wave Project (JONSWAP)*, Ergänzungsheft zur Deutschen Hydrographischen Zeitschrift, Reihe A(8^o), No. 12

Hasselmann, K., D.B. Ross, P. Muller and W. Sell (1976), *A parametric wave prediction model*, Journal of Physical Oceanography, Vol. 6, No. 2, pp. 200-228

Hasselmann, D.E., M. Dunckel and J.A. Ewing (1980), *Directional wave spectra observed during JONSWAP 1973*, Journal of Physical Oceanography, Vol. 10, No. 8, pp. 1264-1280

Holthuijsen, L.H., M.Tienstra and G.J.v.d.Vliet (1974), *Stereophotography of the Sea Surface, an Experiment*, Proceedings of the International Symposium on Ocean Wave Measurement and Analysis, American Society of Civil Engineers, pp. 153-169

Holthuijsen, L.H. (1978), *Preliminary results of some stereophotographic sorties flown over the sea surface*, Proceedings 12th Symposium on Naval Hydrodynamics, National Academy of Sciences, Washington, D.C., 1979, pp. 555-569

Holthuijsen, L.H. (1979), *Stereophotography of ocean waves*, communications on Hydraulics, Report No. 79-1, Department of Civil Engineering, Delft University of Technology

Horikawa, K. and T. Sasaki (1972), *Field observation of nearshore current system*, Proceedings 13th Coastal Engineering Conference, pp. 635-652, Vancouver, Canada

Howard, C.D.D. (1969), *Photogrammetric measurement of directional wave spectra*, Underwood McLellan & Associates Ltd. and Western Photogrammetry Ltd. and Government Department of Public Works, Pierson, W.J. and L. Moskowitz (1964), *A proposed spectral form for fully developed wind seas based on the similarity theory of S.A. Kitaigorodskii*, Journal of Geophysical Research, Vol. 69, No. 24, pp. 5181-5190

Regier, L.A. and R.E. Davies (1977), *Observations of the power and directional spectrum of ocean surface waves*, Journal of Marine Research, Vol. 35, No. 3, pp. 433-451

Schuhmacher, A. (1939), *Stereophotogrammetrische Wellenaufnahmen*, Wiss. Ergeb. Deutschen Atlantischen Expedition auf dem Forschungs und Vermessungsschiff "Meteor" 1925-1927, Oceanographische Sonderuntersuchungen, Erste Lieferung, Berlin

Schwidefsky, K. (1963), *Grundriss der Photogrammetrie*, 6 Auflage, Teuber Verlagsgesellschaft, Stuttgart

Seymour, R.J. (1977), *Estimating wave generation on restricted fetches*, Proc. ASCE, Journal Waterway, Port, Coastal and Ocean Division, Vol. 103, No. WW2, paper 12924, pp. 251-264

Simpson, L.S. (1967), *Preliminary investigation of the directional spectrum of ocean wave height as obtained from stereo wave photographs*, Ocean Dynamics Branch, Exploratory Oceanography Division, Research and Development Department, U.S. Naval Oceanographic Office, Washington, D.C., Informal Manuscript No. 67.1

Singleton, R.C. (1969), *An Algorithm for computing the Mixed Radix Fast Fourier Transform*, IEEE Transactions on Audio and Electroacoustics, Vol. AU-17, No. 2, pp. 93-103

Stewart, R.H. and C.C. Teague (1980), *Decameter radar observations of ocean wave growth and decay*, Journal of Physical Oceanography, Vol. 10, No. 1, pp. 128-143

Stilwell, D. (1969), *Directional energy spectra of the sea from photographs*, Journal of Geophysical Research, Vol. 74, No. 8, pp. 1974-1986

Sugimori, Y. (1975), *A study of the application of the holographic*

Appendix I Altitude of photography

The altitude of a photographic mission is chosen on the basis of two considerations. The first consideration concerns the error in the measurements (noise), the second concerns the size of the area to be photographed.

The maximum altitude of photography is related to noise considerations. For conventional geodetic survey the measurement error is estimated as in equation (1) where σ_ε is the standard deviation of the error ε and h is the altitude of photography.

$$\sigma_\varepsilon \simeq 10^{-4}\ h \qquad (1)$$

For stereophotography of the sea surface, where high grade pictures are not expected considering the type of "terrain", a standard deviation three times as large is anticipated, equation (2)

$$\sigma_\varepsilon \simeq 3.10^{-4}\ h \qquad (2)$$

A widely used parameter to quantify the relative importance of noise is the noise-signal ratio. In this case the appropriate entity is the ratio of the variance of the measurement error, σ_ε^2, and the variance of the waves, m_o. Accepting a maximum noise level of 10% of the wave variance, it follows that the maximum altitude of photography (denoted by h_{max}) is given by equation (3).

$$h_{max} \simeq 1000\ m_o^{\frac{1}{2}} \qquad (3)$$

Relating the maximum altitude of photography to the significant wave height H_s by equating m_o to $1/16\ H_s^2$ results in equation (4).

$$h_{min} = \frac{n}{k_m} \frac{f}{0.6\ l'_x} \tag{9}$$

The limitations on the altitude of photography expressed in equations (4) and (9) can be combined into equation (10)

$$\frac{n}{k_m} \frac{f}{0.6\ l'_x} < h < 250\ H_s \tag{10}$$

Before determining the altitude of photography in an actual photographic operation with a given camera system, it is apparently necessary to estimate k_m and H_s.

If the wave field to be photographed is being generated by the local wind it is possible to express k_m in terms of the windspeed U as a relevant parameter in equation (10). For the operational procedures this seemed to be more convenient. For these sea states the dimensionless wavenumber $\tilde{k}_m$ $(=k_m U^2/g)$ and the dimensionless significant waveheight $\tilde{H}_s$ $(=gH_s/U^2)$ are related as in equation (11), e.g. Hasselmann et al. (1976).

$$\tilde{k}_m = p\ \tilde{H}_s^q \tag{11}$$

where p and q are constants. Using dimensionless representations for $\tilde{h}$ and $\tilde{H}_s$, equation (10) can be written as equation (12) where $\tilde{h} = gh/U^2$.

$$\frac{n}{p} \frac{f}{0.6\ l'_x} \tilde{H}_s^{-q} < \tilde{h} < 250\ \tilde{H}_s \tag{12}$$

To estimate the values of p and q, the JONSWAP relationships (Hasselmann et al., 1973) can be used and $p = 1.57 \times 10^{-2}$ and $q = -1.32$ are found. With these values of the constants substituted

Appendix II The least-squares method

If the $\cos^{2s}(\theta/2)$-model were a linear function in terms of the model parameters s and $\bar{\theta}$, one could find the minimum of V_1 (defined in paragraph 3.5.2) by evaluating the first derivatives of equations (1) and (2) which would result in two simple linear equations.

$$\frac{\partial V_1}{\partial \bar{\theta}} = 0 \tag{1}$$

$$\frac{\partial V_1}{\partial s} = 0 \tag{2}$$

But the $\cos^{2s}(\theta/2)$-model is nonlinear in s and $\bar{\theta}$ and a numerical search procedure is used to find the minimum of V_1. A brief description of this procedure follows and it will appear that it may well be called a telescopic search method. No effort was made to investigate other methods which may be more superior in performance.

The value of V_1 is computed for a large number of values of s and $\bar{\theta}$. The minimum value of V_1 and its location in the s,$\bar{\theta}$-plane is identified by scanning V_1 as a function of $\bar{\theta}$ and s. The search is carried out as follows. On the interval $0 < s \leqslant 10$ and $0 \leqslant \bar{\theta} < \pi$, V_1 is computed on a grid of 5 x 5 equidistant points. Scanning this grid provides a rough estimate of the location of a minimum of V_1. The mesh-size of the grid is then taken half the original size and the search area is centered at the location of the minimum found before (the number of gridpoints remains at 5 x 5). The values of V_1 at this new grid are determined and scanned and a more accurate estimate of the location of the minimum of V_1 is obtained. The procedure of decreasing the mesh-size and shifting the centre of the grid is repeated until the location of the minimum shifts less than 5° in $\bar{\theta}$ and less

Appendix III Geophysical conditions

1. Introduction

To evaluate the stereophotographic observations, information is required of the windfield prior to and during the observation and of the topography of the sites. In addition to this it is deemed appropriate to compare the stereophotographic data with independent wave observations at sea level. This requires not only observations of the waves but also information on the tidal currents.

The methods of observation, the analysis and the results of the observations are presented in this Appendix. The information relates to the five spectra addressed in paragraph 5.2 and also to another spectrum (a testcase) not addressed there. The reasons for including a testcase are pointed out in paragraph 4.8. It appears that the geophysical conditions for this testcase are not interesting from a scientific point of view and in this Appendix only scant attention is paid to it.

2. Topography of the sites

The observations were carried out at three locations, two off the Dutch coast and one in the German Bight. (fig. III.2.1).

The first site to be described is located west of the town of Noordwijk off the coast of Holland. A detailed map of this region is given in fig. III.2.2 where the locations of four stereophotographic observations off Noordwijk are indicated (numbers 1 through 4). The longitude and latitude of these locations are given in table III.2.1. It appears that the coast is relatively smooth and slightly concave (as

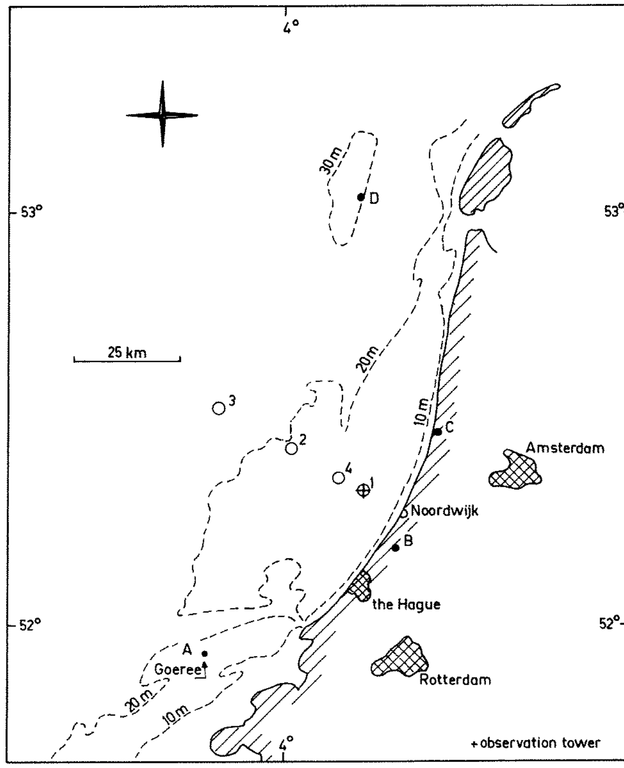

Fig. III.2.2. *Location of the wave observations (numbers 1, 2, 3 and 4 and the test case (Goeree)) and the wind observations (letters A, B, C and D) near Noordwijk.*

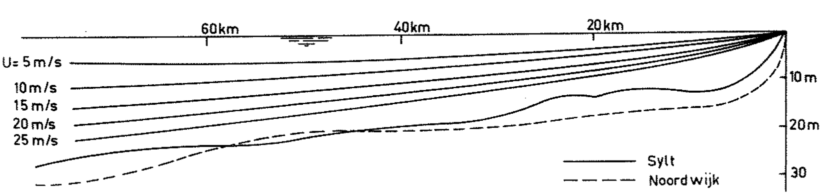

Fig. III.2.3. *Bottom profiles perpendicular to the coast at the Noordwijk site and the Sylt site, lines indicate deep water limit.*

similarity applies to the coastal region of Sylt only (40 km north-south, say). On a larger dimension the coast is irregular and asymetric. It is indented by small openings between islands and in particular by the Elbe and Weser estuaries to the south (fig. III.2.4). Therefore, on a dimension of 150 km north-south, say, this coast differs considerably in geometry from the coast of Noordwijk.

Site	Observation number	Location	Distance off-shore (km)
Noordwijk	1	52^{o} 16' 40" N 04^{o} 17' 24" E	10
Noordwijk	2	52^{o} 22' 25" N 04^{o} 02' 06" E	30
Noordwijk	3	52^{o} 27' 50" N 03^{0} 46' 30" E	50
Noordwijk	4	52^{o} 18' 40" N 04^{o} 10' 30" E	16.5
Sylt	5	55^{o} 02' 30" N 07^{o} 37' 00" E	46.2
Goeree	testcase	52^{o} 55' 50" N 03^{o} 39' 50" E	-

Table III.2.1. Geographic locations of the stereophotographic observatior

3 Meteorological conditions

Three stereophotographic observations were carried out during one flight. The three other observations were obtained during different flights on different days. Consequently four meteorological situations are described here. The sequence corresponds to the sequence of the site descriptions. The time sequence of the observations was different

The observations were carried out with a cup anemometer which was placed at the indicated position (+ 23 m mean sea level) just prior to or after each photographic mission. The direction of the wind was estimated from a wind cone which was permanently available at the tower in the immediate vicinity of the anemometer. Its direction was estimated by visual comparison with the magnetic compass of one of the helicopters (which landed on the platform).

To obtain an estimate of the windspeed and direction at 10 m above mean sea level (which is a commonly used elevation) undisturbed by the tower, two corrections are carried out: one related to the disturbance of the free flow due to the presence of the structure and one related to the wind profile of the free flow. The influence of the bulk of the tower is estimated from experiments with a scale model of this tower in a windtunnel (Maur, 1976). Results of these experiments are available at a point close to the point of observation and these are used for the correction. The correction for elevation is carried out only for the windspeed with the assumed logarithmic wind profile of equation (1) (e.g. Pierson, 1964).

$$U_z = U_{10}\left(1 + \frac{C_{10}^{\frac{1}{2}}}{\kappa} \ln \frac{z}{10}\right) \qquad (1)$$

In this equation C_{10} is the drag coefficient defined as:

$$C_{10} = \frac{\tau}{\rho U_{10}^2}$$

τ is the turbulent shear stress at the surface and ρ is the mass density of air. The value of C_{10} is taken to be 1.5×10^{-3}. The

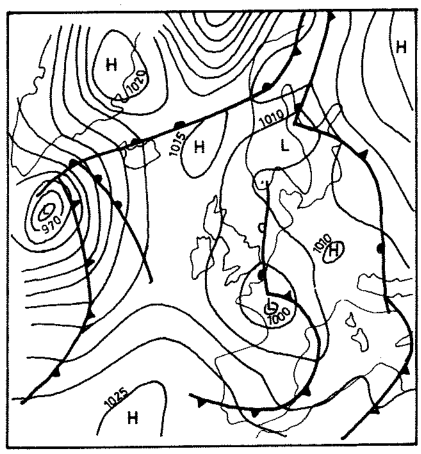

Fig. III.3.3. Weather map of Friday, November 12th, 1976, 12.00 GMT.

The synoptic stations which are closest to the observation site are indicated in fig. III.2.2 by the letters A, B, C and D. In addition to the synoptic stations in the area the research tower was used to obtain wind data. The time history of the hourly synoptic observations during the twelve hours prior to the flight is given in figs. (III.3.4) and (III.3.5). The wind observation at the tower during the photographic operations has also been indicated. A spatial impression of the wind observations at 12.00 GMT is given in fig. (III.3.6).

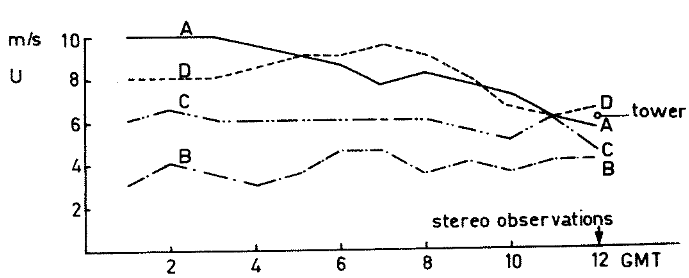

Fig. III.3.4. Windspeed at stations A, B, C and D (fig. III.2.2) on November 12th, 1976 (hourly observations).

been backing at all stations, slightly faster at stations A and C than at stations B and D. The observations at the tower ($U = 6.0$ m/s and $\theta_u = 140^o$) agree with the synoptic observation.

The wind observations in the two hours previous to the observations (the period most relevant for the wave observation) differ from each other by as much as 2.5 m/s in speed and by as much as 50^o in direction. These differences are large but in the area relevant to the stereophotographic observations they are not considered large enough to discredit the situation as inhomogeneous.

In view of the above description of the windfield and in view of the fact that the wind direction at the tower differ only 20^o from the ideal off-shore wind direction (which is 120^o at this site), this situation is labeled as an ideal situation.

Stereophotographic observation number 4, at the Noordwijk site, was obtained on March 23rd, 1976 at approximately 11.20 GMT. Again synoptic information of the Royal Netherlands Meteorological Institute is used to assess the large scale weather pattern (fig. III.3.7, III.3.8). This

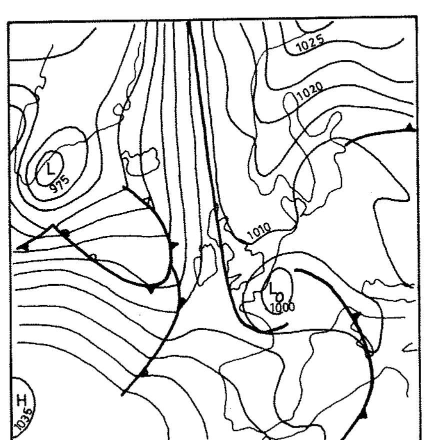

Fig. III.3.7. Weather map of Tuesday, March 23rd, 1976, 0.00 GMT.

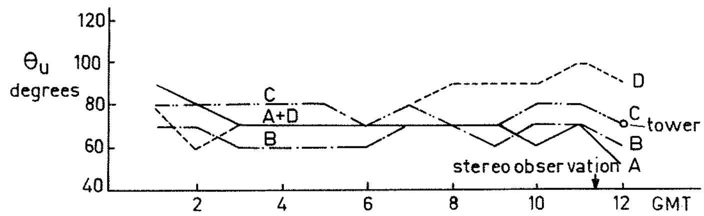

Fig. III.3.10. Wind direction at stations A, B, C and D (fig. III.2.2) on March 23rd, 1976 (hourly observations).

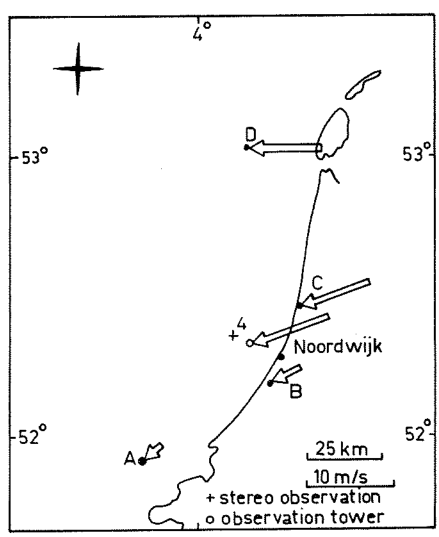

Fig. III.3.11. Wind speed and direction at stations A, B, C and D and at the tower on March 23rd, 1976 at 12.00 GMT.

fied as an ideal situation. However, after an inspection of the wave observation it was found that the coast should be considered on a larger scale than initially assumed (see site description and also the discussion in chapter 5) and the situation was re-labeled as a situation with a homogeneous, stationary windfield with an irregular coast.

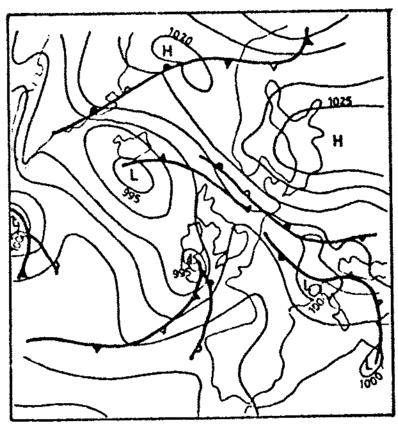

Fig. III.3.12. Weather map of Wednesday, September 18th, 1973, 12.00 GMT.

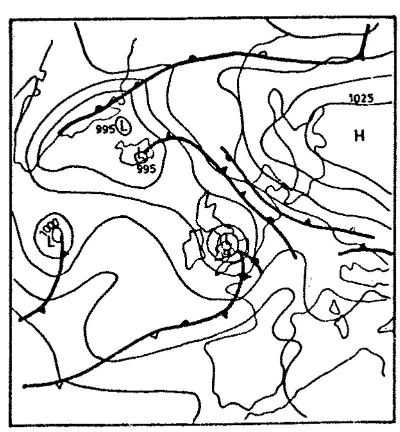

Fig. III.3.13. Weather map of Wednesday, September 19th, 1973, 0.00 GMT.

For the sites off the coast of Holland the maps and tables of the Hydrographic Service in the Netherlands are used (anonymous, 1972, 1975 and 1976). The information in these maps and tables are interpolated to estimate the speed and direction of the tidal currents.

The information for estimating the tidal currents off Sylt was retrieved from the JONSWAP information bank. This information is based on tidal maps and tables of the German Hydrographic Institut and is only available at station E (fig. III.2.4). The tidal map of the Netherlands Hydrographic Service (anonymous, 1976) is used to find the corresponding tidal current at the location of the observation. The current is corrected for wind influence with an empirical factor as suggested in one of the tidal current atlases (anonymous, 1976). This factor indicates that the wind generates a current with a speed of 2% of the windspeed and that the direction of the generated current is about 10 degrees veered with respect to the direction in which the wind blows. The result is presented below.

Site	Observation number	estimates from tidal maps		correction for wind		final estimates	
		V (m/s)	θ_v^o	V (m/s)	θ_v^o	V (m/s)	θ_v^o
Noordwijk	1	0.40	35	0.10	150	0.40	50
Noordwijk	2	0.45	30	0.10	150	0.40	40
Noordwijk	3	0.50	25	0.10	150	0.40	40
Noordwijk	4	0.20	210	0.20	90	0.20	155
Sylt	5	0.20	300	0.20	120	0.00	-
Goeree	testcase	0.80	40	0.20	30	0.90	30

Table III.3.1. Estimated tidal currents during the wave observations. For site and observation number see table III.2.1.

was dropped from the analysis for reasons given in paragraph 4.6 and the assessment is not carried out. Instead, the statements made above for observation number 1 are used to find an indication of a lower limit of the resolution and of the reliability. Due to the statistical dependency between the "raw" spectra the resolution is larger than the gridsize used in the $\vec{k}$-plane. This is indicated in table 4.4.1. The ratio between the data in the non-overlapping areas and the data in all areas was 500/593 and the reliability would increase proportional to the reciprocal of this ratio if the resolution is not affected. However, the resolution is influenced (for the worse) and the reliability is consequently better. This is also indicated in table 4.4.1.

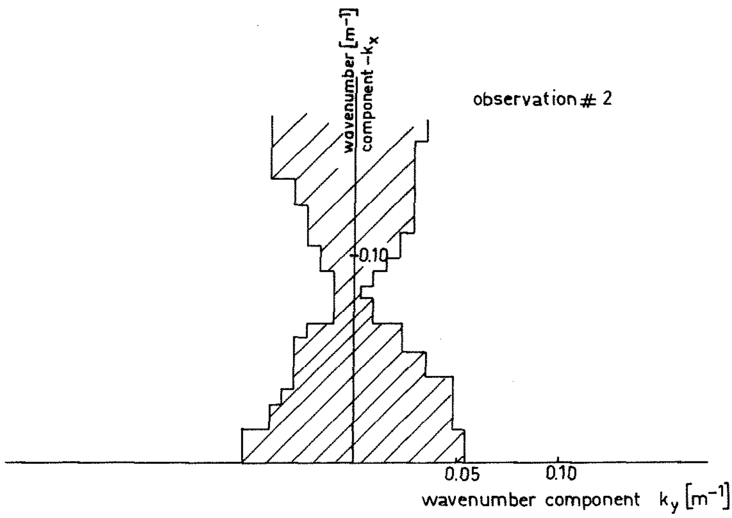

Fig. V.2. Swell and noise areas in observation 2.

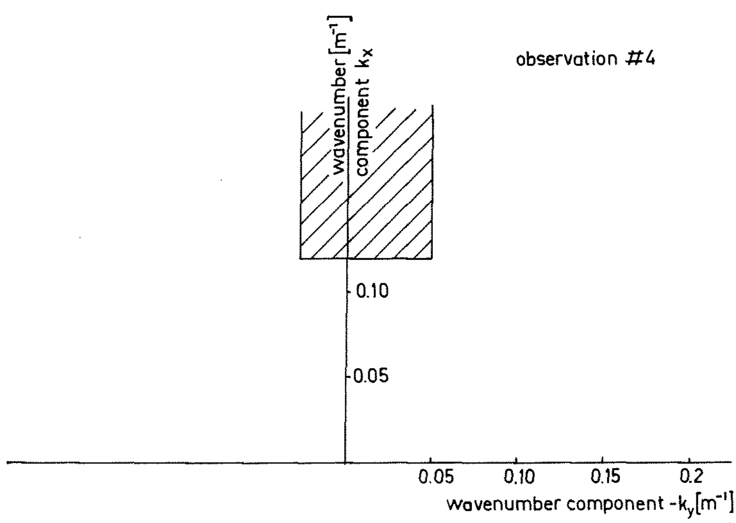

Fig. V.3. Noise area in observation 4.

Appendix VI Values of $\bar{\theta}$ and s

The values of the main direction $\bar{\theta}$ and the width parameter s of the $\cos^{2s}(\theta/2)$-model obtained from the observations are listed below.

wavenumber $k = n\,\Delta k$ where $n = 1,2,\ldots\ldots$
direction $\bar{\theta}$ in degrees from true North

	observation 1			observation 2			observation 4			observation 5		
Δk	54.0 m^{-1}			156.0 m^{-1}			170.0 m^{-1}			220.0 m^{-1}		
k_m	10.8 m^{-1}			15.6 m^{-1}			38.0 m^{-1}			53.4 m^{-1}		
s_m	6.3			4.3			29.7			6.1		
n	$\bar{\theta}$	s	remarks	$\bar{\theta}$	s	remarks	$\bar{\theta}$	s	remarks	$\bar{\theta}$	s	remarks
1	-	-	swell			swell	39	2.1		-	-	noise
2	-	-	swell			swell	03	3.4		-	-	noise
3	147	2.6				swell	00	10.9		135	3.8	
4	133	4.7				swell	05	24.6		129	6.1	
5	129	6.3	peak			swell	13	28.7		135	5.4	
6	136	5.6				swell	15	27.4		121	4.5	
7	134	3.4		-	-	noise	21	17.4		115	4.0	
8	133	3.8		-	-	noise	32	13.1		114	2.8	
9	142	3.6		-	-	noise	37	9.5		125	2.0	
10	147	2.5		145	4.3	peak	40	6.0		128	2.0	
11	146	2.3		135	4.0		40	5.6		120	2.3	
12	156	2.3		136	3.6		54	5.1		95	1.5	
13	167	2.7		130	3.0		59	5.2		-	-	no fit
14	169	2.2		123	3.2		64	4.8		158	1.5	
15	174	2.4		130	2.5		61	3.9		191	1.4	
16	-	-	noise	130	2.1		65	3.8		215	1.7	
17	-	-	noise	133	2.2		64	4.0		183	1.6	
18	-	-	no fit	125	2.1		65	3.4		-	-	noise
19				128	2.1		66	3.2		-	-	noise
20				123	1.9		68	3.2		-	-	noise
21				137	1.7		76	2.9		-	-	noise
22				138	2.2		64	3.1		-	-	noise
23				120	1.9		68	2.3				
24				123	1.7		73	2.2				
25				-	-	no fit	75	2.2				
26				-	-	no fit	68	2.3				
27							68	2.1				
28							88	1.6				
29							70	1.8				
30							93	1.5				
31							100	1.7				
32							78	1.7				
33							-	-	no fit			
34							-	-	no fit			
$\sqrt{20}$							10	29.7	peak			
$\sqrt{17}$										129	6.1	peak

The spectra of fig. VII.1 were found but the agreement with the observations was not satisfactory. Much better agreement was found when using a windspeed of 15 m/s instead of the observed windspeed of 13 m/s, particularly for the most outward station, fig. VII.2. Since it appeared to be possible to hindcast these spectra fairly well with a 15 m/s windspeed, this procedure was used to hindcast the spectrum at the location where the pictures were taken. The spectrum thus hindcasted is presented in fig. 4.8.3.

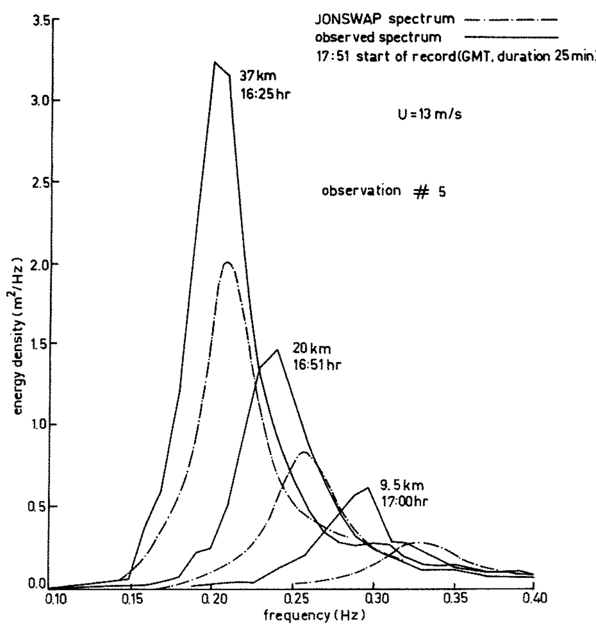

Fig. VII.1. Observed and hindcasted frequency spectra for observation 5, U = 13m/s.

Appendix VIII Testcase

The stereo pictures of the testcase were obtained off the coast of Holland near lightplatform Goeree off the Rhine estuary, fig. III.2.2 of Appendix III. The longitude and latitude are given in table VIII.1. The geometry of the coastline is not relevant for this observation because the observed wavefield was probably not affected by the coastline. The waterdepth is approximately 19 m around the platform and increases gradually to the north and to the west. The 30 m depthline is located approximately 175 km north from the platform (running east-west) and approximately 100 km west from the platform (running north-south).

The pictures were taken on April 19th, 1973 at approximately 10:20 GMT. Synoptical information from the Royal Netherlands Meteorological Institute indicates that the wavefield which was observed was generated by a storm in the northen North Sea and one may well consider the observed waves to be swell. The scientific interest for the present study is therefore marginal and a further assessment of the meteorological situation seems unnecessary. This observation has been added only because it could be compared with an observation at sea level (paragraph 4.8).

The two-dimensional wavenumber spectrum is illustrated in fig. VIII.1. All other information for this testcase is provided in table VIII.1 which corresponds to tables in chapter 4 and Appendix III where similar information is given for the other stereophotographic observations.

time	19-04-1973
	10.20 GMT
location	52^{o} 55' 50" N
	03^{o} 39' 50" E
tidal current	
tidal map V	0.80 m/s
θ_v	40^{o}
wind corr. V	0.20 m/s
θ_v	30^{o}
final est. V	0.90 m/s
θ_v	30^{o}
photo analysis	
app. altitude	300 m
camera type	Hasselblad
direction of y-axis	360^{o}
area size	130 x 130 m^2
number of areas	10
mesh-size	6.5 x 6.5 m^2
% zero's	0
spectral analysis	
degrees of freedom per estimate	20
peak wavenumber	$(130.0)^{-1}$ m^{-1}
directional resolution	
at $k = k_m$	64^{o}
at $k = 2\ k_m$	35^{o}

Table VIII.1. Characteristics of the testcase.

$\sigma = \sigma_a$ for $f<f_m$ $\quad \sigma = \sigma_b$ for $f>f_m$

$$\sigma_a = 0.184 \tanh[5.3\times10^{-5}(\tilde{x} - 35800)] + 0.21 \quad (6)$$

$$\sigma_b = 0.239 \tanh[5.3\times10^{-5}(\tilde{x} - 35800)] + 0.28 \quad (7)$$

where $\tilde{x} = gx/U^2$, with x the distance to shore, g the gravitational acceleration and U the windspeed, $\tilde{f}_m = Uf_m/g$ with f_m the frequency at the peak of the spectrum.

However, when the significant waveheight (H_s) is computed from these relationships (with $H_s = 4\sqrt{m_o}$, where m_o is the integral over the frequency spectrum from $f = 0$ to $f = 3f_m$) as a function of fetch it is found that its overshoots its value for very large fetches. This is illustrated in fig. IX-1 in dimensionless form.

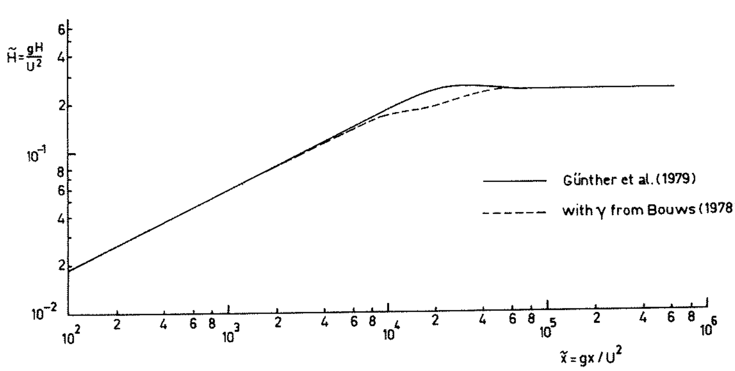

Fig. IX.1. Dimensionless significant waveheight as function of dimensionless fetch.

As such behaviour has never been observed (e.g. Wilson, 1965) and, in fact, the authors were not aware of this behaviour (Günther, 1979) one of the relationships is replaced. This is the relationship for γ because it was also found that the spectral density could obtain a maxi-

$$s' = \left(\frac{3.3 - \gamma_0}{2.3}\right) s_m - \left(\frac{1 - \gamma_0}{2.3}\right) s \qquad (11)$$

where s' is the modified value of s.

The contourlines of the modified spectrum based on this expression for $\beta \simeq 1$ is shown in fig. IX-3.

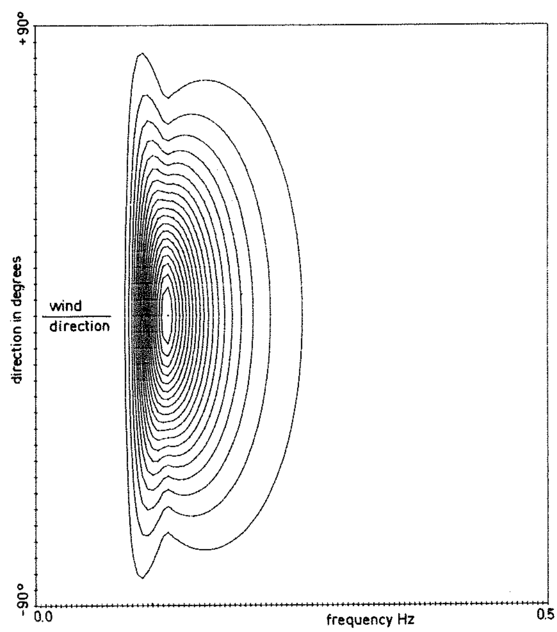

Fig. IX.2. Fully developed two-dimensional spectrum with s from Hasselmann et al. (1980).

Appendix X Hindcasted spectra

The results of the hindcasts in the irregular coast situation and in the slanting wind situation are presented in the format of contour line plots. Numerical information on the energy density is not required as the comparison with the observations relate to the location of peaks and main directions only.

The result of the hindcasted spectrum in the irregular coast situation is shown in fig. X-1. The information in fig. 5.3.2 is taken from this illustration.

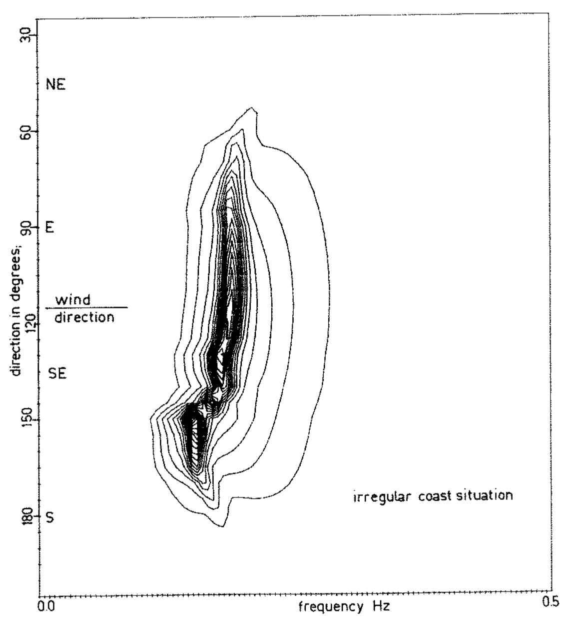

Fig. X.1. Hindcasted two-dimensional spectrum for observation 5.

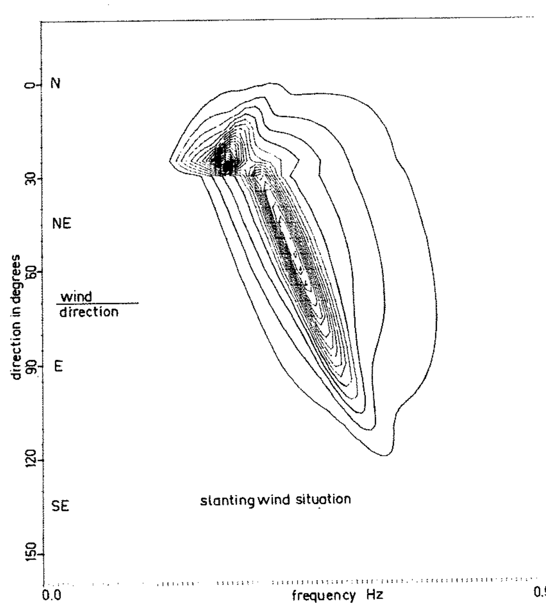

Fig. X.3. Hindcasted two-dimensional spectrum for observation 4.